Reactivation of intrabasement structures during rifting: A case study from offshore Norway

Thomas B. Phillips [1]*, Christopher A-L. Jackson [1], Rebecca E. Bell [1], Oliver B. Duffy [2], Haakon Fossen [3]

***Corresponding author: t.phillips13@imperial.ac.uk**

[1] Basins Research Group (BRG), Department of Earth Science and Engineering, Imperial College, South Kensington Campus, Prince Consort Road, London, SW7 2BP, UK

[2] Bureau of Economic Geology, Jackson School of Geosciences, The University of Texas at Austin, University Station, Box X, Austin, TX 78713-8924, USA

[3]Department of Earth Science/Natural History Collections, University of Bergen, Allégaten 41, 5008 Bergen, Norway

Abstract

Pre-existing structures within crystalline basement may exert a significant influence over the evolution of rifts. However, the exact manner in which these structures reactivate and thus their degree of influence over the overlying rift is poorly understood. Using borehole-constrained 2D and 3D seismic reflection data from offshore Southern Norway we identify and constrain the three-dimensional geometry of a series of enigmatic intrabasement reflections. Through 1D waveform modelling and 3D mapping of these reflection packages, we correlate them to the onshore Caledonian thrust belt and Devonian shear zones. Based on the seismic-stratigraphic architecture of the post-basement succession we identify several phases of reactivation of the intrabasement structures associated with multiple tectonic events. Reactivation preferentially occurs along relatively thick (c. 1km), relatively steeply

dipping (c. 30°) structures, with three main styles of interactions observed between them and overlying faults: (i) faults exploiting intrabasement weaknesses represented by intra-shear zone mylonites; (ii) faults that initiate within the hangingwall of the shear zones, inheriting their orientation and merging with said structure at depth; or (iii) faults that initiate independently from and cross-cut intrabasement structures. We demonstrate that large-scale discrete shear zones act as a long-lived structural template for fault initiation during multiple phases of rifting.

1. Introduction

Continental rifting is often considered in terms of extension of relatively homogeneous lithosphere (Gupta et al., 1998; Cowie et al., 2000; Gawthorpe and Leeder, 2000). However, continental lithosphere is considerably more complex than envisaged in these idealised models, typically containing a range of structures imparted by previous tectonic events. These structures span a range of scales; from large-scale crustal sutures and orogenic belts (Daly et al., 1989; Mogensen and Korstgård, 2003; Paton and Underhill, 2004; Bird et al., 2014; Bladon et al., 2015), pre-existing fault populations and outcrop-scale fault and fracture networks (Kirkpatrick et al., 2013; Whipp et al., 2014; Duffy et al., 2015), to structures formed at the grain- and even micro-scale. Such pre-existing heterogeneities may; i) reactivate during later tectonic events; ii) act as nucleation sites for later rift-related faults; and iii) localise and modify the regional stress field, thus fundamentally modifying the physiography and evolution of overlying rifts. Field, seismic and potential field data indicate that the reactivation of intrabasement structures may influence the development of rift systems (Daly et al., 1989; Fraser and Gawthorpe, 1990; Maurin and Guiraud, 1993; Ring, 1994; Færseth, 1996; Clemson et al., 1997; Morley et al., 2004; Paton and Underhill, 2004; Gontijo-Pascutti et al., 2010; Bellahsen et al., 2013; Bird et al., 2014; Whipp et al., 2014; Salomon et al., 2015; Scheiber et al., 2015), an observation further supported by numerical

and analogue modelling (Huyghe and Mugnier, 1992; Faccenna et al., 1995; Bellahsen and Daniel, 2005; Henza et al., 2011; Autin et al., 2013; Chattopadhyay and Chakra, 2013; Tong et al., 2014). However, many of these relationships between intrabasement structure and rift systems are simply based on plan-view correlations, with little consideration given to their three-dimensional geometric relationships or kinematic interactions, primarily due to difficulties in imaging and constraining the 3D geometry of the intrabasement structure. For instance, in seismic reflection data, crystalline basement often appears acoustically transparent due to typically low internal impedance contrasts and large burial depths. Although intrabasement structures have previously been imaged using deep seismic reflection data (Chadwick et al., 1983; Choukroune, 1989; Abramovitz and Thybo, 2000; Hedin et al., 2012; Fossen et al., 2014), these studies have sparse data coverage and are unable to resolve the required detail and 3D geometry of said strucutres, particularly at upper crustal levels. In addition, interpretations based upon potential field data may be non-unique and of relatively low resolution, with these data typically unable to image discrete structures. In contrast, discrete structures can be analysed in some detail in the field, although these data may not be of sufficient extent to permit truly three-dimensional analysis of large-scale structure.

Recent advances in the quality of seismic data have allowed for the detailed mapping of intrabasement structures on both 2D (Bird et al., 2014) and 3D (Reeve et al., 2013; Bird et al., 2014) seismic reflection data, and it has been demonstrated that these structures can both influence (Bird et al., 2014) or not influence (Reeve et al., 2013) the structural style and evolution of later rift systems. Therefore, the selective reactivation of intrabasement structures may depend on physical and geometric properties related to their formation and composition, as well as their relation to regional stress fields imposed during later tectonic events. A detailed understanding of the overall 3D geometry and internal architecture of

intrabasement structures is therefore vital to determine the controls on their selective reactivation and how this affects the geometry and evolution of the overlying rift.

In this study we use closely spaced 2D and 3D seismic reflection data from offshore SW Norway (Figure 1, 2) to constrain the 3D geometry of a series of enigmatic reflection packages within crystalline basement, along with key stratigraphic horizons in the overlying rift. Being located close to the margin of the North Sea rift basin and having experienced a complex tectonic history (Figure 3), crystalline basement in the study area is located at relatively shallow depths (<4.5 km) and is highly heterogeneous, containing a series of prominent coherent reflections that can be mapped across large parts of the seismic data. We observe two types of discrete reflection packages within crystalline basement: i) thin (c. 100 m) reflection packets displaying a concave-upwards geometry (Figure 4); and ii) thicker (c. 1.5 km) reflection packages of inclined reflectivity that dip at c. 30° (Figure 4). Through 1D waveform modelling, we show that these reflections originate from a layered sequence, which we propose are layered intra-shear zone mylonites. Furthermore, because the study area is located close to the Norwegian coastline (Figure 1), we are able to confidently link these reflections to the previously mapped and established onshore geology, specifically shear zones associated with the Caledonian Orogeny and the Devonian orogenic collapse (Morley, 1986; Pedersen and Hertogen, 1990; Fossen and Rykkelid, 1992; Gabrielsen et al., 2002; Fossen, 2010; Roffeis and Corfu, 2013; Corfu et al., 2014).

Based upon our seismic interpretation of both the cover and the basement, we observe a range of interactions between the intrabasement structures and the overlying rift-related faults throughout multiple tectonic events. In some instances reactivation of intrabasement structures has a profound effect on the later rift; whereas in others, rift-related faults form independently of intrabasement structure. As such, we investigate the factors controlling this

selective reactivation of the intrabasement structures and offer insights into the mechanisms of their reactivation.

2. Geological Setting

2.1 Regional setting

This study focuses on a 20,000 km^2 area located offshore SW Norway, encompassing the WNW- trending Egersund Basin, the N-trending Åsta Graben (Figure 1), and the Stavanger Platform (Figure 1). The major basement-involved faults in the study area are the Åsta Fault, and the Stavanger and Sele High Fault Systems, bounding the Åsta Graben, Stavanger Platform and Sele High respectively (Figure 1). The Stavanger Fault System (SFS) consists of two NW-to-NNW striking fault segments (Figure 1). The Åsta fault strikes N-S along the eastern margin of the Åsta Graben. Between the Åsta and Stavanger fault systems, the south-western margin of the Stavanger Platform is bordered by a shallowly dipping ramp, herein termed the Stavanger Ramp (Figure 1). The N-S striking Sele High Fault System (SHFS) forms the western boundary to the Åsta Graben and the Egersund Basin (Figure 1).

2.2 Geological History

The present day crystalline basement of the North Sea largely formed during the Late Ordovician-Early Devonian Caledonian orogeny (McKerrow et al., 2000) (Figure 3), with older Proterozoic basement remnant to the east of the study area. The Scandian phase of the Caledonian orogeny involved continent-continent collision between Laurentia to the west and Baltica in the east. During this collision, allochthonous material was transported ESE onto the margin of Baltica along a basal zone of mechanically weak Cambrian shales and phyllites overlain by a package of highly sheared rocks of Baltican origin, collectively referred to as the basal décollement zone (Figure 1) (Fossen, 1992; Milnes et al., 1997). The Caledonian

Deformation Front (CDF) represents the easternmost limit of Caledonian allocthonous material. The in-situ CDF is preserved along eastern Norway, whereas post Caledonian erosion across large parts of southern Norway results in the westward translation of the CDF as observed today (Huuse, 2002; Japsen et al., 2002). Hence, the original CDF can only approximately be located in the area covered by Figure 1. In this study, we refer to the CDF as the present, erosional boundary between Caledonian allochthonous material and Proterozoic autochthonous crystalline basement (Figure 1).

Caledonian shortening was succeeded by Devonian orogen-scale extension (McClay et al., 1986; Dewey, 1988; Fossen, 1992)(Figure 3). Extension was initially accommodated by the reactivation of pre-existing Caledonian structures (Mode I reactivation of Fossen et al., 1992), most notably the basal décollement, as indicated onshore by asymmetric mylonitic fabrics and the overprinting of top-to-SE by top-to-NW shear sense indicators (Fossen, 1992). This reversal of shear along Caledonian structures accounted for 20-30 km of extension across Norway before these structures became locked at low angles. Subsequent extension was accommodated by the formation of large-scale through-going extensional shear zones (Mode II reactivation of Fossen et al., 1992) and a series of Devonian basins (Fossen, 2010; Vetti and Fossen, 2012). The extensional shear zones are mapped onshore across southern Norway to the northern margin of the study area along the present coastline (Pedersen and Hertogen, 1990; Fossen, 2010; Bøe et al., 2011). These shear zones are typically 1-2 km thick, with some up to 5 km (Fossen and Hurich, 2005).

Extension in the Carboniferous-Early Permian, potentially in response to post-Variscan orogenic collapse (Ziegler, 1992), resulted in the formation of a number of major faults, notably the Sele High and Stavanger fault systems (Sørensen et al., 1992; Jackson and Lewis, 2013; Jackson and Lewis, 2015) (Figure 1). Subsequent post-rift thermal subsidence led to the formation of the North and South Permian basins, which, during the Late Permian

were filled with the evaporite-dominated Zechstein Supergroup (Ziegler, 1992). During the Mesozoic, the North Sea experienced two main rift phases, the first occurring during the Late Permian-Early Triassic in response to the breakup of Pangea. E-W-directed extension (Coward et al., 2003; Fossen et al., 2016) led to the development of a predominately N-trending rift (Ziegler, 1992; Odinsen et al., 2000), the formation of the Åsta fault, and the reactivation of other major faults within the study area (Sørensen et al., 1992; Jackson and Lewis, 2013; Jackson and Lewis, 2015). A second rift phase lasted from the Late Jurassic into the Early Cretaceous, with previous studies suggesting an extension direction of either E-W (Bartholomew et al., 1993; Brun and Tron, 1993; Bell et al., 2014) or WNW-ESE to NW-SE (Færseth, 1996; Doré et al., 1997; Færseth et al., 1997). Rifting resulted in the initiation of new faults and the reactivation of some pre-existing faults (Bell et al., 2014), including a number of those located within the study area (Figure 3). This rift phase occurred in response to the collapse of a Middle Jurassic Mid-North Sea Dome (Underhill and Partington, 1993), which broadly coincided with the opening of the Norwegian Sea - North Atlantic rift system (Ziegler, 1992). Following Late Jurassic-to-Early Cretaceous rifting, a protracted period of post-rift thermal subsidence was interrupted during the Late Cretaceous by mild inversion related to the Alpine orogeny (Figure 3) (Biddle and Rudolph, 1988; Cartwright, 1989; Jackson et al., 2013).

3. Dataset and methodology

Key horizons and structures were mapped on a closely spaced (maximum 5 km spacing) grid of 2D seismic reflection data (imaging to 7-9 s two-way-travel time, TWT), and a 3600 km^2 3D dataset with 25 m line spacing (imaging to 5 s TWT) (Figure 2). Seismic reflection data are zero-phase and displayed following the SEG reverse polarity convention; i.e. a downward increase in acoustic impedance is represented by a trough (red) and a downward decrease in acoustic impedance is represented by a peak (black) (Figure 5). The ages of key seismic

horizons were constrained using 17 boreholes, three of which penetrate crystalline basement (Figure 3). Checkshot data from these wells were used to create a velocity model to convert structural measurements from the time to depth domain.

The dominant intrabasement frequency within the 2D seismic data is c. 20 Hz; using an interval velocity of 6100 ms^{-1} for crystalline basement (Abramovitz and Thybo, 2000), we estimate an intrabasement vertical resolution of c. 80 m. The quality of imaging within basement is generally very good, although it deteriorates towards the SE due to thicker Zechstein salt in the eastern Egersund Basin. Intrabasement reflections were mapped, where possible, within the 3D volume and across individual closely spaced 2D lines. The distinct seismic expression of the larger intrabasement features (Figure 5, 6) allowed for correlation between individual 2D lines, allowing them to be mapped over a larger area and to greater depths than permitted by the 3D volume alone (Figure 3).

Seismic-scale variations in crystalline basement lithology typically produce small impedance contrasts, due to minor differences in seismic velocity and density, and do not produce prominent reflections in seismic reflection data. Therefore, in conjunction with the typically large burial depths of crystalline basement beneath rifts, intrabasement structures are often poorly resolved on seismic reflection data (Torvela et al., 2013). However, imaging of crystalline basement may be improved within areas of shallow basement. In addition, intrabasement reflectivity may be enhanced through constructive interference within layered sequences, such as those observed between highly strained mylonite zones and less deformed country rock (Fountain et al., 1984; Wang et al., 1989).

1D waveform modelling was used to test the geological origin of the characteristic reflection patterns observed within the intrabasement structures. We make no attempt to model the absolute or relative amplitudes of the data, instead focussing on the interference between

reflections and the first-order reflection patterns. In addition, we do not account for attenuation of the seismic wave with depth. Reflection co-efficients of +1 and -1 were assumed for increases and decreases in acoustic impedance respectively. Taking into account the reverse data polarity, we use an incident negative ricker wavelet of 20 Hz, assuming an intrabasement velocity of 6100 ms^{-1}. Wavelet responses were calculated from horizons at varying depths and then convolved to produce the overall model reflection pattern.

4. Interpretation of intrabasement structure

4.1 Offshore intrabasement reflectivity

We observe two types of prominent reflections within crystalline basement: i) relatively thin (c. 80-100 m), concave-upwards, high-amplitude reflection packets that dip 0-10° and are characterised by a trough-peak-trough wavetrain (Figure 4a); and ii) relatively thick (c. 1-2 km) packages of high-amplitude reflectivity dipping at c. 30°, which are herein termed intrabasement packages (IP) (Figure 4a). In detail, the IP comprise an anastomosing network of high-amplitude, sub-parallel reflections (Figure 4a, 5). Although the overall geometry of the IP, i.e. the top and base of the packages, can be mapped across multiple 2D seismic sections (Figure 6, 7), we are unable to map individual internal reflections as they are often laterally discontinuous (Figure 6).

Basement-penetrating wells (Figure 2) sample Caledonian and Proterozoic crystalline basement, confirming that the mapped deep reflectivity is within crystalline basement. The geometry and extent of the reflections do not mimic that of any reflections in the overlying cover, thus we argue they are not multiples (Figure 5). Furthermore, the intrabasement

reflections are visible across independent seismic datasets, suggesting that they represent real geological boundaries rather than an acquisition- or processing-related geophysical artefact.

4.2 Waveform modelling of intrabasement reflections

Later in this paper, we correlate the large scale intrabasement packages described above to discrete basement shear zones that are mapped onshore southern Norway. However, we first here use 1D waveform modelling to demonstrate that the observed reflection patterns resemble the general internal geometries of shear zones described elsewhere.

1D waveform modelling allows us to recreate first-order reflection patterns observed in the data. First, we find that the observed first-order reflection pattern, the characteristic trough-peak-trough wavetrain, cannot be generated using a single interface, instead forming through constructive interference between reflections generated within a layered sequence (Figure 4b). We therefore produce a series of layered models with different layer and interlayer thicknesses (Fountain et al., 1984) and compare these to the observed reflection patterns (Figure 4b). A reflection coefficient of -1 was used to define the top of a layer, and +1 used to define the base (Figure 4b).

Our analyses show that reflections produced by closely spaced (c. 100 m) layers constructively interfere to create a trough-peak-trough wavetrain, similar to the thin reflection packets observed within the data (Figure 4a,b). We find that the observed intrabasement reflection patterns are best represented by c. 100 m thick layers of material with a lower acoustic impedance (AI) separated by 50-100 m of higher acoustic impedance material. In the example shown in Figure 4b, 100 m thick low-AI layers, separated by 50 m thick, high-AI layers best fit the upper segment of the observed reflection pattern, whereas a high-AI layer thickness of 100 m best fits the lower part. Furthermore, we find that continually adding similarly spaced layers to the sequence acts to increase the number of cycles present in, and

therefore the overall thickness of, the overall reflection package, resembling the observed IPs (Figure 4a,b). As the spacing between layers increases, the degree of constructive interference decreases until two distinct reflections can be resolved. At a spacing of >150 m, layers begin to produce two distinct reflection events (Figure 4b), as opposed to constructively interfering within one another. Slight variations in layer and interlayer thicknesses result in differing degrees of interference, causing variations in the imaging of individual layered sequences. Prominent reflections within the package may represent areas displaying the optimal spacing (c. 50-100 m) for constructive interference, with less distinct reflections generated at non-optimal layer and interlayer thicknesses.

Based on our modelling results we propose that the observed intrabasement structures most likely represent intra-shear zone mylonites. Previous studies have also correlated similar structures observed in seismic reflection data, showing the characteristic trough-peak-trough wavetrain, to mylonite zones as observed onshore (Fountain et al., 1984; Hurich et al., 1985; Reeve et al., 2013), with some offering direct control through outcrop and well data (Wang et al., 1989; Hedin et al., 2012; Lorenz et al., 2015). In addition, our observed thicknesses of c. 100 m are of a similar scale to those proposed in previous modelling studies (Fountain et al., 1984; Reeve et al., 2013), and the internal structure of these intra-shear zone mylonites display a similar anastomosing geometry to those observed elsewhere; for example, onshore Norway (Boundy et al., 1992; Scheiber et al., 2015), the central alps (Choukroune and Gapais, 1983), the Cap de Creus shear zone network (Druguet et al., 1997; Carreras, 2001; Carreras et al., 2010; Ponce et al., 2013) and southern Africa (Goscombe et al., 2003; Goscombe and Gray, 2008; Rennie et al., 2013). However, we must also consider that the observed 100 m scale mylonites only reflect one scale of localisation present within shear zones (Carreras, 2001); the top and base of thicker mylonite zones may not constructively interfere and produce a prominent seismic reflection, whereas thinner mylonite zones may

not be resolved in our seismic data. The modelled mylonite zones may actually represent a high concentration of thinner mylonite layers, at thicknesses below seismic resolution and therefore producing the same reflection pattern as a thicker mylonite zone (Carreras, 2001).

4.3 Geometry of offshore intrabasement structures

Having modelled the reflection patterns within the intrabasement reflection packages and having argued that these may be linked to intra-shear zone mylonites (Figure 4b), we now provide a more detailed description of the overall geometry of the discrete reflection packages in order to link them explicitly to specific basement structures mapped onshore. A series of thin reflection packets are observed above a shallowly dipping intrabasement package, termed IP1 (Figure 5, 6). IP1 is in turn is cross-cut by other intrabasement packages, termed IP2 and IP3 (Figure 5). A further intrabasement package, IP4 is observed further to the south (Figure 6, 7).We now describe the 3D geometry of these intrabasement packages.

IP1 is 0.5-1 s TWT (c. 1 km) thick and is the lowermost intrabasement package mappable within the study area. IP1 predominately dips 0° to 11° W, although it may locally dip shallowly to the east, and is truncated by the top basement unconformity beneath the Stavanger Platform (Figure 5, 6). To the north of the study area, beneath the Stavanger Platform, IP1 is cross-cut by intrabasement structures IP2 and IP3 (Figure 5). IP1 is not visible to the west and in the hanging wall of IP2. To the south, IP1 is mapped beneath the Egersund Basin and Flekkefjord High (Figure 1), within the hanging wall of the Sele High Fault System, where it is slightly offset by IP4 (Figure 7, 8). Across the Stavanger platform, a series of relatively thin (100 ms or c. 100 m) reflection packets are locally mapped (over c. 750 km^2; Figure 9). These reflections sole-out onto IP1, strike N-S and dip westwards at 0-10°, displaying a concave-upwards geometry. When viewed collectively they exhibit a flat-ramp style geometry (Figure 6).

IP2 is 1-1.5s TWT (c. 2 km) thick. Along the western margin of the Stavanger Platform it is truncated along the top basement unconformity, where it strikes N-S and dips c. 30° W (Figure 5). Here, IP1 is present in the footwall but not the hangingwall of IP2. Further south, beneath the Stavanger ramp and Egersund Basin, IP2 strikes NE-SW before being offset by c. 2 s TWT by the N-S striking Sele High Fault System (Figure 9). Along the northern part of the Sele High Fault System, IP2 is truncated by the top basement unconformity in the hanging wall of the fault; whereas in the centre it is offset and is present on both sides of the fault, and in the south it is only present within the footwall (Figure 8). In the south, where IP2 is only present in the footwall of the Sele High Fault System, IP1 is not offset, and is present within the hanging wall of IP2 and the hanging wall of the Sele High Fault System.

IP3 is 1-1.5 s TWT (c. 2 km) thick and is truncated at the top basement unconformity across the Stavanger Platform (Figure 5). IP3 strikes roughly N-S, dips c. 30° W, and also offsets IP1 (Figure 5). A local basin, herein termed the Stavanger Basin, is present above the structure (Figure 5). Limited data coverage across the Stavanger Platform does not allow for detailed mapping of the package, although it is observed along strike further to the south along the southern margin of the Stavanger Platform and the Stavanger Fault System (Figure 7).

A further intrabasement structure, IP4, splays-off southwards from IP2, beneath the Egersund Basin and Flekkefjord High. This IP is 0.5-1 s (0.5-1 km) thick, strikes 010° N and dips 30° W (Figure 6, 7, 8). IP4 also offsets IP1 and may merge with IP2 at depth (Figure 6) and along strike to the north (Figure 9). East of IP4, several other IPs are observed in, and possibly splay off from, the hanging wall of the larger structure (Figure 8). These may represent additional IPs splaying from IP4, mirroring the geometric relationship of IP2 and IP4 further to the north (Figure 7); or alternatively, a segment of IP1 within the footwall of IP4.

4.5. Onshore-offshore correlation of intrabasement structures

Based on our waveform modelling showing that the intrabasement reflections represent intra-shear zone mylonites (Figure 4), and combined with their overall 3D geometry, we now link our offshore intrabasement structures to specific shear zones mapped onshore. In particular, we link them to the CDF and Devonian extensional shear zones that have previously been studied and mapped in great detail (Figure 1) (Fossen, 1992; Fossen and Dunlap, 1998; Gabrielsen et al., 2002; Olesen et al., 2004; Bingen et al., 2008; Bøe et al., 2011; Lundmark et al., 2013; Roffeis and Corfu, 2013).

The subcrop of IP1 at top crystalline basement correlates along strike northwards to the CDF onshore. In addition, basement-penetrating wells (18/11-1; Figure 9) sample Caledonian crystalline basement (Sørensen et al., 1992) west of IP1, and a Proterozoic granite to the east (10/5-1; Figure 9), indicating that the CDF must lie between these locations (Figure 9). Based on our seismic mapping of IP1, and supported by these observations and the 1D waveform modelling, we interpret IP1 to represent the offshore continuation of the basal décollement zone of the Caledonian thrust belt, with the subcrop at top basement level representing the CDF itself. To the south, our interpretation of the CDF correlates along strike to the location of the CDF in the Central North Sea as mapped using deep regional seismic data (Abramovitz and Thybo, 1999; Abramovitz and Thybo, 2000), overall extending the mapped extent of this structure over 100 km into the Central North Sea (Figure 9). A number of thin intra-shear zone mylonites are observed above the basal décollement (Figure 10). Based on their low dip (0-10°) and overall flat-ramp geometry, we infer that these structures initially formed as mylonitic Caledonian thrusts (cf. Reeve et al. (2013)).

A series of intrabasement packages (IP2-4), dipping at c. 30°, cross-cut the shallowly dipping basal décollement of the Caledonian thrust belt (Figure 5, 6, 9). IP2 correlates along-strike to

the Devonian-aged extensional Karmøy Shear Zone (KSZ) observed onshore. The KSZ forms a southwards splay from the Hardangerfjord Shear Zone to the north (Fossen, 2010). IP3 is confidently correlated c. 30 km along-strike to the onshore Stavanger Shear Zone (SSZ). These interpretations are further constrained locally by interpretations of the deep regional ILP seismic data (Fossen et al., 2014). IP4 however, does not correlate to any structures mapped onshore or on deep seismic reflection data; we thus propose that this represents a previously undefined structure that we hereby term the Flekkefjord Shear Zone (FSZ; Figure 9). We infer that the FSZ splays southwards from the footwall of the KSZ, showing a similar relationship to that observed between the KSZ and the Hardangerfjord Shear Zone further north (Figure 9, 11).

We have constrained the 3D geometry of a series of intrabasement structures associated with the Caledonian thrust belt and Devonian extensional shear zones (Figure 9). Caledonian allocthons and the associated basal décollement are observed within the hanging walls of later (i.e. cross-cutting) Devonian extensional shear zones. A number of these shear zones splay southwards, potentially merging at depth and initially originating from the HSZ to the north (Figure 9).

5. Reactivation of intrabasement structures

Using our detailed 3D framework of intrabasement structure, combined with seismic-stratigraphic analysis of the sedimentary cover, we now investigate the reactivation of these structures during post-Devonian tectonic events and examine how this has affected the geometry and evolution of the superposed rift.

5.1. Reactivation of Caledonian thrust structures

We map a series of thin intra-shear zone mylonites, previously interpreted as Caledonian thrusts (Figure 6), above the basal décollement and beneath a series of Lower Permian depocentres (Figure 6, 10). These structures are only mapped locally on the Stavanger Platform (Figure 9); further north, these thin structures are very difficult to identify and map across rather sparse, relatively widely spaced 2D seismic profiles (Figure 2).

Two seismic facies, defining an upper and lower set of depocentres, are observed within the hanging wall of some of the interpreted Caledonian thrusts (Figure 10), indicating some extensional reactivation along these structures. The upper depocentres are typically 2-4 km in diameter and around 100 ms thick (c. 130 m). They display higher amplitudes than the lower depocentres and surrounding seismic facies (Figure 10). The upper depocentres are truncated by the overlying Base Cretaceous Unconformity (BCU) and internal reflections onlap onto the underlying strata (Figure 10). The lower depocentres are truncated and separated from the upper depocentres by an unconformity of unknown age. The lower depocentres are typically of lower amplitude than those above, forming a unit c. 200 ms (c. 300 m) thick, although the boundary with the underlying basement is often unclear (Figure 10). Wedge-shaped stratal geometries are observed locally, thickening towards the Caledonian thrusts (Figure 10).

We interpret that the lower depocentres formed during an early phase of extensional reactivation along the Caledonian thrusts. The age of the strata flanking these structures and therefore the timing of the extensional reactivation of the Caledonian thrusts is unknown due to a lack of well penetration and erosion associated with the BCU (Figure 10). However, these structures may have undergone extensional reactivation during the initial stages of Devonian orogenic collapse (Mode I), when extension was accommodated through backsliding of the orogenic wedge and reactivation of Caledonian structures (Fossen, 1992). During this extension, the mylonitic shear zones may have formed weaknesses within the

nappe sequence, acting to localise strain and preferentially reactivating; leading to the development of the lower depocentres. We speculate that the high-amplitude upper depocentres may have formed during a later period of brittle extension, with the bounding structures, the extensionally reactivated Caledonian thrusts, having been weakened during the first phase of reactivation.

A later phase of reverse reactivation is observed along some of the structures, as indicated by the presence of a raised depocentre bounded by two Caledonian thrusts and an accompanying inversion monocline (Figure 10). The BCU is gently folded across this monocline, indicating the structure is post-Cretaceous in age. We suggest that the causal compressional event may have occurred during the Upper Cretaceous, potentially related to the Alpine inversion (Figure 5) (Biddle and Rudolph, 1988; Cartwright, 1989; Jackson et al., 2013).

As described above, we observe extensional and compressional reactivation of individual Caledonian thrusts. However, the depocentres resulting from this reactivation are relatively minor compared to the main rift-related faults and do not affect the large-scale rift morphology. It appears that Mode I Devonian extension had a negligible impact on the overall evolution of the rift, especially in comparison to the formation of the large-scale Devonian Shear Zones during subsequent Mode II extension, as described below.

5.2. Reactivation of Devonian shear zones

In addition to that described in the previous section, we also observe multiple phases of reactivation of Devonian extensional shear zones. Along the KSZ we observe Triassic strata that thicken across a series of faults rooted into internal planes within the shear zone (Figure 7, 11). In addition, across-fault thickening and wedge-shaped stratal geometries are observed in Triassic strata in the hanging wall of the Flekkefjord Shear Zone (FSZ) (Figure 11). This indicates that both structures underwent extensional reactivation during the Triassic.

Furthermore, a series of salt walls are located above the intrabasement structures in the south (Figure 8); Triassic extensional reactivation of the underlying intrabasement structures may have led to salt mobilisation and the formation of overlying salt walls (Koyi and Petersen, 1992). Jurassic and Lower Cretaceous strata also thicken across the FSZ, though they are largely isopachous across the KSZ. Slight thickening of Lower Cretaceous strata is observed across the KSZ in the Stavanger Ramp area (Figure 11), although the majority of extension in this area was accommodated by the FSZ rather than the KSZ. The KSZ accommodates large amounts of extension in the north beneath the Åsta Graben where the FSZ is not present (Figure 12), whereas to the south extension is initially distributed between the KSZ and FSZ (Figure 7, 11), and then solely accommodated by the FSZ (Figure 8). Bøe et al. (2011) propose further evidence for the Jurassic extensional reactivation of the KSZ, with the Karmsundet Basin, offshore Karmøy island, formed through extensional reactivation of the KSZ.

A NE-facing, NW-SE-striking monocline is observed above the FSZ (Figure 11). Upper Cretaceous strata onlap the forelimb of the monocline, indicating it formed during the Late Cretaceous. Similarly oriented structures are observed in this part of the North Sea (Biddle and Rudolph, 1988; Cartwright, 1989; Thybo, 2000; Jackson et al., 2013). For example, Jackson et al. (2013) observe inversion-related anticlines directly along-strike to the south, above the Stavanger Fault System (Figure 7). These folds initiated during the latest Turonian-to-earliest Coniacian and the Santonian, and were caused by NE-directed compression resulting from the Alpine Orogeny (Jackson et al., 2013). The observed monocline above the FSZ forms a continuation of this structure to the NW, with reactivation occurring along a fault related to the FSZ as opposed to the Stavanger Fault System.

6. Relationships between intrabasement structures and rift-related faults

We note a strong plan-view correlation between the location and orientation of the intrabasement structures at top basement level and the location and orientation of the later rift-related faults (Figure 9). For example, the Stavanger Fault System and the Lista fault blocks follow the same trend as the underlying SSZ and CDF respectively (Figure 9); likewise, the Åsta Fault shares the orientation and polarity of the underlying KSZ (Figure 9). Similar correlations between basement structures and rift-related faults have previously been noted in plan-view (Younes and McClay, 2002; Bellahsen et al., 2013; Fossen et al., 2016), with faults inheriting pre-existing structures that are oriented oblique to the regional stress field. Examining these relationships in cross section, we observe a range of interaction styles between the intrabasement structures and the later rift-related faults: i) 'merging faults' that join along the margin of the shear zone at depth (e.g. between the KSZ and the Åsta fault; Figure 12); ii) 'exploitative faults' that root into internal planes at the underlying shear zone subcrops (e.g. above the FSZ; see Figure 11; and above the SSZ; see Figure 5); and iii) 'cross-cutting faults' that form independently from and are unaffected by any underlying basement structure (e.g. where the Sele High Fault System cross-cuts the KSZ; Figure 13). We here provide detailed descriptions of these three interaction styles between the intrabasement structure and rift-related faults.

6.1 Faults merging along the margin of shear zones at depth

Some rift-related faults are located within the hangingwall of intrabasement structures, following their orientation and dip direction in map view (Figure 9), and merging along the margins of these structures at depth (Figure 12). The upper part of the shear zone subcrops within the footwall of the younger rift-related fault. For example, the Åsta fault is situated above the KSZ, soling down into the margin of the structure at c. 3 s TWT (c. 4 km). Triassic strata are largely restricted to the hanging wall of the Åsta fault, indicating that this structure may have been active during the Permo-Triassic rift event. Jurassic and Lower Cretaceous

strata also thicken across the Åsta fault, indicating that the fault was also active during the Jurassic and Early Cretaceous, and that the KSZ was reactivated during Late Jurassic-Early Cretaceous rifting (Figure 12). In addition, a wedge-shaped package of reflections occurs within the Åsta Graben, with this package truncated along the base Triassic along at its top (Figure 12). We infer this package records a pre-Triassic, potentially Carboniferous-Permian period of extension (Sørensen et al., 1992; Ziegler, 1992).

6.2 Faults exploiting internal planes within shear zones

Some rift-related faults link downward into discrete planes within the intrabasement shear zones, as observed in association with IP4 (Figure 7), the KSZ (Figure 11) and the SSZ (Figure 5). In these instances we infer that reactivation occurs internally within the shear zone, potentially exploiting weak internal mylonite zones, forming a fault that then propagates upwards into the cover. Furthermore, in the locations where the shear zones are truncated at top basement a number of minor depocentres and extensional top-basement offsets are observed, suggesting extension along internal planes within the shear zone (Figure 5, 12).

As previously described, the Stavanger Basin is located within the Stavanger Platform (Figure 1), directly above the Stavanger Shear Zone (Figure 5, 9). Due to a lack of well control across the Stavanger Platform we are unable to directly determine the age of the contained sediments, although a Permo-Triassic rift age seems likely, which is consistent with the Stavanger Fault System along strike to the south (Figure 9). The shear zones offset the basal décollement of the Caledonian thrust belt. A series of faults bound the overlying depocentre and exploit internal planes within the underlying shear zone. In addition, two large lozenge-shaped reflection packages are observed within the shear zone, bound by faults (Figure 5).

To the south, a similar exploitative interaction is proposed for the relationship between the Stavanger Fault System and the SSZ (Figure 9), although this is not as well imaged in our seismic data (Figure 7). The Stavanger Fault System has previously been interpreted to represent a reactivated Caledonian thrust (Sørensen et al., 1992); however, based on our interpretation and mapping of the structure (Figure 9), along with similar relationships observed to the north (Figure 5), we take to be the basal décollement of the Caledonian thrust belt for the southern fault segment (Figure 9), and the SSZ for the northern segment (Figure 6). The presence of Permian Zechstein salt in the area often complicates the stratal geometries; however, where salt is largely absent, we observe that Triassic strata thicken towards the faults, indicating that they were active at this time (Figure 7). In addition, Jackson et al. (2013), observe the formation of an inversion-related anticline above the fault (Figure 7), indicating that the fault, and therefore potentially the SSZ, underwent reverse reactivation during Late Cretaceous compression.

6.3 Faults cross-cutting intrabasement structure

Although many intrabasement structures and rift-related cover structures are often geometrically and kinematically linked, as described in the previous two sections, we also observe instances where the two are seemingly unrelated, with the latter cross-cutting the former. The Sele High Fault System is situated between the subcrops of the KSZ to the east and the HSZ to the northwest. This fault system strikes N-S, and dips c. 60°E. At c. 5 s TWT the fault cross-cuts the underlying KSZ, offsetting the structure by c. 2 s TWT (c. 3.5 km) (Figure 13). A further fault is observed within the footwall of the Sele High Fault System, offsetting an earlier formed, potentially Carboniferous basin (Sørensen et al., 1992), and appearing to terminate at the KSZ (Figure 13).

7. Discussion

7.1 3D Geometry and inter-relationships between intrabasement structures

The Caledonian thrust belt was cross-cut by extensional Devonian shear zones during orogenic collapse of the Caledonides (Fossen, 2010). We observe similar relationships within our data, with the basal décollement of the Caledonian thrust belt being extensionally offset across the SSZ and KSZ, although it is not imaged in the downthrown hanging wall of the latter (Figure 5). Distributed ductile deformation across the Stavanger Shear Zone during its formation resulted in the monoclinal folding of the basal décollement and overlying Caledonian nappes (*sensu* Fossen and Hurich, 2005). Subsequently, during a later, most likely Permo-Triassic rift phase, the SSZ was reactivated in a brittle manner, forming the Stavanger Basin (Figure 5). The Stavanger Basin is bound by faults that exploit internal planes within the shear zone. Contrary to the distributed strain associated with folding of the basal décollement during the Devonian, the brittle faults exploit discrete internal planes within the shear zone; this results in shearing of the basal décollement between these faults, and the development of lozenge-shaped reflection packages (Figure 5) that indicate extensional, sinistral shear (Ponce et al., 2013). Similar relationships are observed onshore; Fossen and Hurich (2005) observe that formation of the Devonian-aged HSZ folded the overlying Caledonian thrust belt. This was later exploited by the overlying brittle Lærdel-Gjende fault system.

The newly defined FSZ forms a southward splay from the KSZ (Figure 9), mirroring the relationship between the latter and the HSZ further to the north. In addition the FSZ merges with the KSZ at depth (Figure 11). Fossen and Hurich (2005) propose that the HSZ represents the boundary between thick-skinned to the north and thin-skinned tectonics towards the south and is associated with a major Moho offset (Fossen et al., 2014). Based on our observations we may speculate that the southwards splaying KSZ and FSZ join the HSZ at mid-crustal depths representing a more thin-skinned component of Devonian orogenic collapse.

7.2 Selective reactivation of intrabasement structure

Using the 3D framework of intrabasement structure along with the seismic stratigraphic architecture of the overlying rift, we are able to examine in detail the interactions between the intrabasement structures and later rift-related faults throughout multiple tectonic events. Our data suggest that thinner (c. 100 m) structures (i.e. Caledonian thrusts) are less likely to interact with later rift-related faults than thicker (1-2 km) structures. Although we do observe minor reactivation of Caledonian thrusts (Figure 10), we suggest this is linked to Mode I Devonian, rather than subsequent Permo-Triassic or Jurassic-Cretaceous extension (Fossen and Rykkelid, 1992), and does not affect the overall geometry and evolution of the superposed rift. Reeve et al. (2013) identify similar reflection packets to the north in the northern North Sea, also interpreting them as Caledonian thrusts, and find that rift-related faults cross-cut and are unaffected by their presence. Similarly, Kirkpatrick et al. (2013) suggest a degree of scale-dependency on the reactivation of intrabasement structures, with large-scale structures preferentially reactivated and smaller structures cross-cut. We argue that thicker structures are preferentially reactivated because they are more likely to contain a layer weak or several weak layers, in this instance represented by intra-shear zone mylonites, that may be reactivated during later rift events (White et al., 1986; Salomon et al., 2015).

Although the mapped intrabasement structures are all relatively low-angle (<30 °), we also note, notwithstanding Devonian mode I extension, a lack of reactivation of the relatively shallow-dipping (c. 10 °), albeit relatively thick (c. 1-2 km) intrabasement structures, such as the basal décollement. Conversely, we observe multiple phases of reactivation along the steeper (c. 30°), relatively thick (c. 1-2 km) Devonian shear zones (Figure 5, 12). Therefore, in addition to thicker structures being preferentially reactivated, we suggest that steeper structures are also preferentially reactivated over shallow ones, in accordance with theoretical considerations (Sibson, 1985). The orientation of intrabasement structures relative

554 to the regional stress field may also play a role in their selective reactivation (Ring, 1994;
555 Morley et al., 2004; Henza et al., 2011), although we are unable to assess this factor as the
556 studied intrabasement structures all roughly trend N-S and dip westward.

557 Finally, we find that previously reactivated structures are consequently weakened and
558 therefore more likely to reactivate during a later tectonic event. For example, IP4 initially
559 formed as an extensional structure during the Devonian, underwent extensional reactivation
560 during Permo-Triassic rifting, was further extensionally reactivated during the Late Jurassic-
561 Early Cretaceous rift phase, and finally underwent reverse reactivation in response to Late
562 Cretaceous compression (Figure 6, 11).

563 **7.3 Fault-intrabasement structure interactions**

564 We observe three main styles of interaction between rift-related faults and underlying
565 Devonian shear zones (e.g. ‘merging’, ‘exploitative’, and ‘cross-cutting’ faults; see Figure
566 14).

567 Exploitative faults are observed along IP4, the KSZ and the SSZ (Figure 5, 8, 9), rooting into
568 internal reflection planes interpreted as layered sequences of highly strained mylonites and
569 relatively undeformed rock. The mylonitic foliation, along with the overall layering, mean the
570 shear zone is strongly mechanically anisotropic, with the mylonite zones being weaker than
571 the surrounding relatively undeformed rocks (White et al., 1980; Chattopadhyay and Chakra,
572 2013). This strong heterogeneity may be preferentially exploited during later brittle
573 reactivation of the shear zones (Gontijo-Pascutti et al., 2010; Salomon et al., 2015; Scheiber
574 et al., 2015). In addition, varying thicknesses of mylonite zones and the degree of strain
575 experienced may have different strengths, providing multiple potential sites for later faults to
576 exploit during brittle reactivation of the shear zones.

The Åsta fault is an example of a merging fault interaction, joining along the margin of the KSZ at depth (Figure 5, 12). What is less clear is where the rift-related fault initiates and how it subsequently propagates, does it initiate at and grow upwards from the shear zone; or nucleate within the hanging wall of the shear zone, before propagating downwards and joining the structure at depth? In the former situation, extension may be accommodated by ductile reactivation of the shear zone at depth, with the formation of a steeper fault becoming preferential at shallower levels (Huyghe and Mugnier, 1992); whilst theoretically possible we note that, at least within the study area, the KSZ does not reach the depths of the ductile regime. In the latter situation, the shear zone acts as an intrabasement heterogeneity, acting to perturb the regional stress field and localise strain, causing fault nucleation within its hanging wall, with these faults inheriting the orientation and dip direction of the underlying structure. Subsequent growth would then cause the faults to physically link with the underlying structure. Furthermore, previous studies have shown that the dip of later rift-related faults may be influenced by the dip of underlying shear zones (Ring, 1994; Salomon et al., 2015), with initial fractures coalescing to produce a steeper through-going fault. Due to the reasons outlined above, we prefer the latter scenario, where faults initiate above and ultimately link downward with the intrabasement structures.

The Devonian shear zones often show rugose top basement subcrops, with minor extensional exploitative faults present (Figure 9). The weak, low-angle shear zone may initially accommodate small amounts of extension, forming exploitative faults (Figure 5, 13). Upon further extension, the low-angle shear zone may become locked, resulting in the formation of a steeper fault within the hanging wall, inheriting the geometric properties of the underlying shear zone, which eventually displays a ‘merging’ relationship (Figure 9).

Cross-cutting faults, such as the Sele High Fault System (Figure 13), form in areas where large intrabasement structures are lacking. Therefore they initiate in a manner similar to faults

forming within homogeneous material (Cowie et al., 2000; Gawthorpe and Leeder, 2000). Such faults form in response to the regional stress field, perpendicular to the extension direction and at typical dips of c. 60°, as opposed to in response to local perturbations surrounding intrabasement structures (Figure 15). As they propagate laterally and vertically the faults are at a high angle to and therefore cross-cut underlying, low-angle intrabasement structures.

7.4 Effects of intrabasement structure on rift geometry and evolution

Rifts forming within relatively pristine (i.e. homogenous) crust are typically characterised by regularly spaced, sub-parallel faults that strike perpendicular to the regional extension direction (Gupta et al., 1998; Cowie et al., 2000; Gawthorpe and Leeder, 2000). However, the geometry and evolution of rift basins in areas of more heterogeneous (i.e. 'non-pristine') crust, such as those containing pre-existing, discrete intrabasement structures, differ from and thus cannot be adequately described using established models of rift evolution. For example, we show that large-scale Devonian shear zones act as heterogeneities within this otherwise 'pristine' crust and, being prone to reactivation, act to locally modify the regional stress field (Figure 15). These structures form a 'template' for fault development and thus the subsequent basin structure associated with later extensional and contractional tectonic events. In addition, the spacing between the reactivated intrabasement structures can also control the degree of faulting that occurs. Closely spaced shear zones are able to host a wider zone of exploitative faulting, with each fault rooted in an individual intra-shear zone mylonite zone. Strain is therefore distributed over a wider area, leading to an overall more gently dipping rift margin (Figure 11). Such a scenario is observed across the Stavanger Ramp (Figure 9), where strain is distributed across a series of relatively low displacement exploitative faults atop the closely spaced KSZ and FSZ (Figure 11). Due to their close-spacing within the overall shear zones, not all of the intra-shear zone mylonites host an exploitative fault. This observation is in

agreement with Sassi et al. (1993), who observe that only selected structures are reactivated when closely spaced.

Where large intrabasement structures are absent, rift-related faults form in response to the regional stress field and cross-cut smaller intrabasement structures (Figure 14). A lack of large, discrete intrabasement structures may help to explain the lack of fault-intrabasement structures relationships observed in areas where the intrabasement structure is cross-cut (Kirkpatrick et al., 2013; Reeve et al., 2013). Alternatively, such structures may be present in other rifts, but are not imaged in seismic reflection data or resolved in potential field data.

8. Conclusions

Using closely spaced 2D and 3D seismic data we have resolved the 3D geometry of a series of spectacularly imaged structures within crystalline basement over a 10,000 km^2 area offshore southern Norway. These structures are correlated onshore, and are analysed in context to the evolution and geometry of the overlying rift. Throughout this study, we have shown that:

1. The characteristic reflection geometries of the intrabasement structures cannot be generated by a single interface within crystalline basement. 1D waveform modelling suggests that this forms through constructive interference between layers roughly 100 m thick separated by 50-100 m. These layers may represent anastomosing mylonite zones separated by relatively undeformed material, as observed in shear zones onshore.

2. Through along-strike correlations to established onshore structures, the observed intrabasement structures represent the offshore continuations of the Caledonian thrust belt and a series of Devonian extensional shear zones. The locations and 3D geometry of these structures are constrained for over 100 km offshore beneath the North Sea rift. A further

650 shear zone, the Flekkefjord Shear Zone is newly defined and mapped offshore. The Devonian
651 shear zones offset the Caledonian thrust belt and in some cases are linked in 3D.

652 3. Selective reactivation of intrabasement structures occurs during later tectonic events,
653 exerting a strong influence over the evolution and geometry of the overlying rift. Thicker,
654 steeper structures, such as the Devonian shear zones, are preferentially reactivated at the
655 expense of thinner, more gently-dipping structures. Previously reactivated, and therefore
656 weaker, structures are then preferentially reactivated during later tectonic events.

657 4. We observe a number of interactions between the reactivated Devonian shear zones and
658 the later rift-related faults: i) Faults that form within the hanging wall of intrabasement shear
659 zones due to local stress perturbations and merge with the structures at depth; ii) faults that
660 exploit internal weaknesses, i.e. mechanical anisotropies exhibited by mylonites, within the
661 shear zones; and iii) faults that form independently away from intrabasement structure in
662 response to the regional stress field, and cross-cut underlying structure. Close proximity
663 between intrabasement structures allows strain to be distributed over a wider area, resulting in
664 multiple, low-displacement faults, and an overall gentler rift margin.

665 5. The presence of large-scale intrabasement structures acts to locally modify the regional
666 stress field, and exhibits a first-order control on the location of later rift-related faults, with
667 basin-bounding faults inheriting this pre-existing framework. Rift-related faults form in
668 response to the regional stress field in areas where this pre-existing framework is not present.
669 Characteristics such as anomalous fault geometries and local areas of distributed faulting may
670 be used to infer the presence of an underlying complexity, such as a discrete intrabasement
671 structure, especially in areas where crystalline basement is poorly imaged.

672 The geometry and distribution of underlying basement heterogeneities dictates the location of
673 many basin margins, determining the initial rift physiography and size (Figure 14). In

addition, the repeated reactivation of these structures shows how they play a long-lived role in the evolution of the rift system throughout multiple tectonic events.

Acknowledgments

The authors would like to thank PGS and TGS for allowing us to show the seismic data used in this study, along with Schlumberger for providing academic licences for use of Petrel software. This contribution forms part of the MultiRift Project funded by the Research Council of Norway's PETROMAKS programme (Project number 215591) and Statoil to the University of Bergen and partners Imperial College, University of Manchester and University of Oslo.

References

Abramovitz, T., Thybo, H., 1999. Pre-Zechstein structures around the MONA LISA deep seismic lines in the southern Horn Graben area. Bulletin of the Geological Society of Denmark 10, 99-116.

Abramovitz, T., Thybo, H., 2000. Seismic images of Caledonian, lithosphere scale collision strucutres in the southeastern North Sea along Mona Lisa Profile 2. Tectonophysics 317, 27-54.

Autin, J., Bellahsen, N., Leroy, S., Husson, L., Beslier, M.-O., d'Acremont, E., 2013. The role of structural inheritance in oblique rifting: Insights from analogue models and application to the Gulf of Aden. Tectonophysics 607, 51-64.

Bartholomew, I.D., Peters, J.M., Powell, C.M., 1993. Regional structural evolution of the North Sea: oblique slip and the reactivation of basement lineaments. Geological Society, London, Petroleum Geology Conference series 4, 1109-1122.

Bell, R.E., Jackson, C.A.L., Whipp, P.S., Clements, B., 2014. Strain migration during multiphase extension: observations from the northern North Sea. Tectonics.

Bellahsen, N., Daniel, J.M., 2005. Fault reactivation control on normal fault growth: an experimental study. Journal of Structural Geology 27, 769-780.

Bellahsen, N., Leroy, S., Autin, J., Razin, P., d'Acremont, E., Sloan, H., Pik, R., Ahmed, A., Khanbari, K., 2013. Pre-existing oblique transfer zones and transfer/transform relationships in continental margins: New insights from the southeastern Gulf of Aden, Socotra Island, Yemen. Tectonophysics 607, 32-50.

Biddle, K.T., Rudolph, K.W., 1988. Early Tertiary structural inversion in the Stord Basin, Norwegian North Sea. Journal of the Geological Society 145, 603-611.

Bingen, B., Nordgulen, Ø., Viola, G., 2008. A four-phase model for the Sveconorwegian orogeny, SW Scandinavia. Norwegian journal of Geology 88, 43-72.

Bird, P.C., Cartwright, J.A., Davies, T.L., 2014. Basement reactivation in the development of rift basins: an example of reactivated Caledonide structures in the West Orkney Basin. Journal of the Geological Society 172, 77-85.

Bladon, A.J., Clarke, S.M., Burley, S.D., 2015. Complex rift geometries resulting from inheritance of pre-existing structures: Insights and regional implications from the Barmer Basin rift. Journal of Structural Geology 71, 136-154.

712 Bøe, R., Fossen, H., Smelror, M., 2011. Mesozoic sediments and structures onshore Norway and in
713 the coastal zone. Norges geologiske undersøkelse Bulletin 450.
714 Boundy, T.M., Fountain, D.M., Austrheim, H., 1992. Structural development and petrofabrics of
715 eclogite facies shear zones, Bergen Arcs, western Norway: implications for deep crustal
716 deformational processes. Journal of Metamorphic Geology 10, 127-146.
717 Brun, J.-P., Tron, V., 1993. Development of the North Viking Graben: inferences from laboratory
718 modelling. Sedimentary Geology 86, 31-51.
719 Carreras, J., 2001. Zooming on Northern Cap de Creus shear zones. Journal of Structural Geology 23,
720 1457-1486.
721 Carreras, J., Czeck, D.M., Druguet, E., Hudleston, P.J., 2010. Structure and development of an
722 anastomosing network of ductile shear zones. Journal of Structural Geology 32, 656-666.
723 Cartwright, J.A., 1989. The kinematics of inversion in the Danish Central Graben. Geological Society,
724 London, Special Publications 44, 153-175.
725 Chadwick, R.A., Kenolty, N., Whittaker, A., 1983. Crustal structure beneath southern England from
726 deep seismic reflection profiles. Journal of the Geological Society 140, 893-911.
727 Chattopadhyay, A., Chakra, M., 2013. Influence of pre-existing pervasive fabrics on fault patterns
728 during orthogonal and oblique rifting: An experimental approach. Marine and Petroleum Geology
729 39, 74-91.
730 Choukroune, P., 1989. The ECORS Pyrenean deep seismic profile reflection data and the overall
731 structure of an orogenic belt. Tectonics 8, 23-39.
732 Choukroune, P., Gapais, D., 1983. Strain Patterns in Rocks Strain pattern in the Aar Granite (Central
733 Alps): Orthogneiss developed by bulk inhomogeneous flattening. Journal of Structural Geology 5,
734 411-418.
735 Clemson, J., Cartwright, J., Booth, J., 1997. Structural segmentation and the influence of basement
736 structure on the Namibian passive margin. Journal of the Geological Society 154, 477-482.
737 Corfu, F., Andersen, T.B., Gasser, D., 2014. The Scandinavian Caledonides: main features, conceptual
738 advances and critical questions. Geological Society, London, Special Publications.
739 Coward, M.P., Dewey, J.F., Hempton, M., Holroyd, J., 2003. Tectonic evolution, in: Evans, D.,
740 Graham, C., Armour, A., Bathurst, P. (Eds.), The Millenium Atlas: petroleum geology of the central
741 and northern North Sea, Geological Society of London.
742 Cowie, P.A., Gupta, S., Dawers, N.H., 2000. Implications of fault array evolution for synrift depocetre
743 development: insights from a numerical fault growth model. Basin Research 12, 241-261.
744 Daly, M.C., Chorowicz, J., Fairhead, J.D., 1989. Rift basin evolution in Africa: the influence of
745 reactivated steep basement shear zones. Geol Soc London, Special Publication 44, 309-334.
746 Dewey, J.F., 1988. Extensional collapse of orogens. Tectonics 7, 1123-1139.
747 Doré, A.G., Lundin, E.R., Fichler, C., Olesen, O., 1997. Patterns of basement structure and
748 reactivation along the NE Atlantic margin. Journal of the Geological Society 154, 85-92.
749 Druguet, E., Passchier, C.W., Carreras, J., Victor, P., den Brok, S., 1997. Analysis of a complex high-
750 strain zone at Cap de Creus, Spain. Tectonophysics 280, 31-45.
751 Duffy, O.B., Bell, R.E., Jackson, C.A.L., Gawthorpe, R.L., Whipp, P.S., 2015. Fault growth and
752 interactions in a multiphase rift fault network: Horda Platform, Norwegian North Sea. Journal of
753 Structural Geology 80, 99-119.
754 Faccenna, C., Nalpas, T., Brun, J.-P., Davy, P., Bosi, V., 1995. The influence of pre-existing thrust faults
755 on normal fault geometry in nature and in experiments. Journal of Structural Geology 17, 1139-1149.
756 Færseth, R.B., 1996. Interaction of Permo-Triassic and Jurassic extensional fault-blocks during the
757 development of the northern North Sea. Journal of the Geological Society 153, 931-944.
758 Færseth, R.B., Knudsen, B.E., Liljedahl, T., Midbøe, P.S., Søderstrøm, B., 1997. Oblique rifting and
759 sequential faulting in the Jurassic development of the northern North Sea. Journal of Structural
760 Geology 19, 1285-1302.
761 Fossen, H., 1992. The role of extensional tectonics in the Caledonides of south Norway. Journal of
762 Structural Geology 14, 1033-1046.

763 Fossen, H., 2010. Extensional tectonics in the North Atlantic Caledonides: a regional view. Geological
764 Society, London, Special Publications 335, 767-793.
765 Fossen, H., Dunlap, J.W., 1998. Timing and kinematics of Caledonian thrusting and extensional
766 collapse, southern Norway: evidence from 40Ar/39Ar thermochronology. Journal of Structural
767 Geology 20, 765-781.
768 Fossen, H., Gabrielsen, R.H., Faleide, J.I., Hurich, C.A., 2014. Crustal stretching in the Scandinavian
769 Caledonides as revealed by deep seismic data. Geology 42, 791-794.
770 Fossen, H., Hurich, C.A., 2005. The Hardangerfjord Shear Zone in SW Norway and the North Sea: a
771 large-scale low-angle shear zone in the Caledonian crust. Journal of the Geological Society 162, 675-
772 687.
773 Fossen, H., Khani, H.F., Faleide, J.I., Ksienzyk, A.K., Dunlap, W.J., 2016. Post-Caledonian extension in
774 the West Norway–northern North Sea region: the role of structural inheritance. Geological Society,
775 London, Special Publications 439.
776 Fossen, H., Rykkelid, E., 1992. Postcollisional extension of the Caledonide orogen in Scandinavia:
777 Structural expressions and tectonic significance. Geology 20, 737.
778 Fountain, D.M., Hurich, C.A., Smithson, S.B., 1984. Seismic reflectivity of mylonite zones in the crust.
779 Geology 12, 195.
780 Fraser, A.J., Gawthorpe, R.L., 1990. Tectono-stratigraphic development and hydrocarbon habitat of
781 the Carboniferous in northern England. Geological Society, London, Special Publications 55, 49-86.
782 Gabrielsen, R.H., Braathen, A., Dehls, J., Roberts, D., 2002. Tectonic Lineaments of Norway.
783 Norwegian journal of Geology 82, 153-174.
784 Gawthorpe, R.L., Leeder, M.R., 2000. Tectono-sedimentary evolution of active extensional basins.
785 Basin Research 12, 195-218.
786 Gontijo-Pascutti, A., Bezerra, F.H.R., Terra, E.L., Almeida, J.C.H., 2010. Brittle reactivation of mylonitic
787 fabric and the origin of the Cenozoic Rio Santana Graben, southeastern Brazil. Journal of South
788 American Earth Sciences 29, 522-536.
789 Goscombe, B., Hand, M., Gray, D., 2003. Structure of the Kaoko Belt, Namibia: progressive evolution
790 of a classic transpressional orogen. Journal of Structural Geology 25, 1049-1081.
791 Goscombe, B.D., Gray, D.R., 2008. Structure and strain variation at mid-crustal levels in a
792 transpressional orogen: A review of Kaoko Belt structure and the character of West Gondwana
793 amalgamation and dispersal. Gondwana Research 13, 45-85.
794 Gupta, S., Cowie, P.A., Dawers, N.H., Underhill, J.R., 1998. A mechanism to explain rift-basin
795 subsidence and stratigraphic patterns through fault-array evolution. Geology 26, 595-598.
796 Hedin, P., Juhlin, C., Gee, D.G., 2012. Seismic imaging of the Scandinavian Caledonides to define ICDP
797 drilling sites. Tectonophysics 554–557, 30-41.
798 Henza, A.A., Withjack, M.O., Schlische, R.W., 2011. How do the properties of a pre-existing normal-
799 fault population influence fault development during a subsequent phase of extension? Journal of
800 Structural Geology 33, 1312-1324.
801 Hurich, C.A., Smithson, S.B., Fountain, D.M., Humphreys, M.C., 1985. Seismic evidence of mylonite
802 reflectivity and deep structure in the Kettle dome metamorphic core complex, Washington. Geology
803 13, 577-580.
804 Huuse, M., 2002. Cenozoic uplift and denudation of southern Norway: insights from the North Sea
805 Basin. Geological Society, London, Special Publications 196, 209-233.
806 Huyghe, P., Mugnier, J.-L., 1992. The influence of depth on reactivation in normal faulting. Journal of
807 Structural Geology 14, 991-998.
808 Jackson, C.A.L., Chua, S.T., Bell, R.E., Magee, C., 2013. Structural style and early stage growth of
809 inversion structures: 3D seismic insights from the Egersund Basin, offshore Norway. Journal of
810 Structural Geology 46, 167-185.
811 Jackson, C.A.L., Lewis, M.M., 2013. Physiography of the NE margin of the Permian Salt Basin: new
812 insights from 3D seismic reflection data. Journal of the Geological Society 170, 857-860.

Jackson, C.A.L., Lewis, M.M., 2015. Structural style and evolution of a salt-influenced rift basin margin; the impact of variations in salt composition and the role of polyphase extension. Basin Research, n/a-n/a.
Japsen, P., Bidstrup, T., Lidmar-Bergström, K., 2002. Neogene uplift and erosion of southern Scandinavia induced by the rise of the South Swedish Dome. Geological Society, London, Special Publications 196, 183-207.
Kirkpatrick, J.D., Bezerra, F.H.R., Shipton, Z.K., Do Nascimento, A.F., Pytharouli, S.I., Lunn, R.J., Soden, A.M., 2013. Scale-dependent influence of pre-existing basement shear zones on rift faulting: a case study from NE Brazil. Journal of the Geological Society 170, 237-247.
Koyi, H., Petersen, K., 1992. Influence of basment faults on the development of salt structures in the Danish Basin. Marine and Petroleum Geology 10, 82-94.
Lorenz, H., Rosberg, J.E., Juhlin, C., Bjelm, L., Almqvist, B.S.G., Berthet, T., Conze, R., Gee, D.G., Klonowska, I., Pascal, C., Pedersen, K., Roberts, N.M.W., Tsang, C.F., 2015. COSC-1 – drilling of a subduction-related allochthon in the Palaeozoic Caledonide orogen of Scandinavia. Sci. Dril. 19, 1-11.
Lundmark, A.M., Saether, T., Sorlie, R., 2013. Ordovician to Silurian magmatism on the Utsira High, North Sea: implications for correlations between the onshore and offshore Caledonides. Geological Society, London, Special Publications.
Maurin, J.-C., Guiraud, R., 1993. Basement control in the development of the Early Cretaceous West and Central African Rift System. Tectonophysics 228, 81-95.
McClay, Norton, M.G., Coney, P., Davis, G.H., 1986. Collapse of the Caledonian orogen and the Old Red Sandstone. Nature 323, 147-149.
McKerrow, W.S., MacNiocaill, C., Dewey, J.F., 2000. The Caledonian Orogeny redefined. Journal of the Geological Society, London 157, 1149-1154.
Milnes, A.G., Wennberg, O.P., Skår, Ø., Koestler, A.G., 1997. Contraction, extension and timing in the South Norwegian Caledonides: the Sognefjord transect. Geol Soc London, Special Publication 121, 123-148.
Mogensen, T.E., Korstgård, J.A., 2003. Triassic and Jurassic transtension along part of the Sorgenfrei-Tornquist Zone in the Danish Kattegat. Geological Survey of Denmark and Greenland Bulletin 1, 439-458.
Morley, C.K., 1986. The Caledonian thrust front and palinspastic restorations in the southern Norwegian Caledonides. Journal of Structural Geology 8, 753-765.
Morley, C.K., Haranya, C., Phoosongsee, W., Pongwapee, S., Kornsawan, A., Wonganan, N., 2004. Activation of rift oblique and rift parallel pre-existing fabrics during extension and their effect on deformation style: examples from the rifts of Thailand. Journal of Structural Geology 26, 1803-1829.
Odinsen, T., Reemst, P., Beek, P.V.D., Faleide, J.I., Gabrielsen, R.H., 2000. Permo-Triassic and Jurassic extension in the northern North Sea: results from tectonostratigraphic forward modelling. Geological Society, London, Special Publications 167, 83-103.
Olesen, O., Smethurst, M.A., Torsvik, T.H., Bidstrup, T., 2004. Sveconorwegian igneous complexes beneath the Norwegian–Danish Basin. Tectonophysics 387, 105-130.
Paton, D.A., Underhill, J.R., 2004. Role of crustal anisotropy in modifying the structural and sedimentological evolution of extensional basins: the Gamtoos Basin, South Africa. Basin Research 16, 339-359.
Pedersen, R.B., Hertogen, J., 1990. Magmatic evolution of the Karmøy Ophiolite Complex, SW Norway: relationships between MORB-IAT-boninitic-calc-alkaline and alkaline magmatism. Contributions to Mineralogy and Petrology 104, 277-293.
Ponce, C., Druguet, E., Carreras, J., 2013. Development of shear zone-related lozenges in foliated rocks. Journal of Structural Geology 50, 176-186.
Reeve, M.T., Bell, R.E., Jackson, C.A.L., 2013. Origin and significance of intra-basement seismic reflections offshore western Norway. Journal of the Geological Society.
Rennie, S.F., Fagereng, Å., Diener, J.F.A., 2013. Strain distribution within a km-scale, mid-crustal shear zone: The Kuckaus Mylonite Zone, Namibia. Journal of Structural Geology 56, 57-69.

Ring, U., 1994. The influence of preexisting structure on the evolution of the Cenozoic Malawi rift (East African rift system). Tectonics 13, 313-326.
Roffeis, C., Corfu, F., 2013. Caledonian nappes of southern Norway and their correlation with Sveconorwegian basement domains. Geological Society, London, Special Publications.
Salomon, E., Koehn, D., Passchier, C., 2015. Brittle reactivation of ductile shear zones in NW Namibia in relation to South Atlantic rifting. Tectonics 34, 70-85.
Sassi, W., Colletta, B., Balé, P., Paquereau, T., 1993. The origin of sedimentary basins: Inferences from quantitative modelling and basin analysis Modelling of structural complexity in sedimentary basins: The role of pre-existing faults in thrust tectonics. Tectonophysics 226, 97-112.
Scheiber, T., Viola, G., Bingen, B., Peters, M., Solli, A., 2015. Multiple reactivation and strain localization along a Proterozoic orogen-scale deformation zone: The Kongsberg-Telemark boundary in southern Norway revisited. Precambrian Research 265, 78-103.
Sibson, R.H., 1985. A note on fault reactivation. Journal of Structural Geology 7, 751-754.
Sørensen, S., Morizot, H., Skottheim, S., 1992. A tectonostratigraphic analysis of the southeast Northern North Sea Basin, in: Larsen, R.M., Brekke, H., Larsen, B.T., Talleraas, E. (Eds.), Structural and Tectonic modelling and its application to Petroleum Geology. Elsevier, Amsterdam, pp. 19-42.
Thybo, H., 2000. Crustal structure and tectonic evolution of the Tornquist Fan region as revealed by geophysical methods. Bulletin of the Geological Society of Denmark 46, 145-160.
Tong, H., Koyi, H., Huang, S., Zhao, H., 2014. The effect of multiple pre-existing weaknesses on formation and evolution of faults in extended sandbox models. Tectonophysics 626, 197-212.
Torvela, T., Moreau, J., Butler, R.W.H., Korja, A., Heikkinen, P., 2013. The mode of deformation in the orogenic mid-crust revealed by seismic attribute analysis. Geochemistry, Geophysics, Geosystems.
Underhill, J.R., Partington, M.A., 1993. Jurassic thermal doming and deflation in the North Sea: implications of the sequence stratigraphic evidence. 337-345.
Vetti, V.V., Fossen, H., 2012. Origin of contrasting Devonian supradetachment basin types in the Scandinavian Caledonides. Geology 40, 571-574.
Wang, C.-Y., Okaya, D.A., Ruppert, C., Davis, G.A., Guo, T.-S., Zhong, Z., Wenk, H.-R., 1989. Seismic reflectivity of the Whipple Mountain shear zone in southern California. Journal of Geophysical Research 94, 2989.
Whipp, P.S., Jackson, C.A.L., Gawthorpe, R.L., Dreyer, T., Quinn, D., 2014. Normal fault array evolution above a reactivated rift fabric; a subsurface example from the northern Horda Platform, Norwegian North Sea. Basin Research.
White, S.H., Bretan, P.G., Rutter, E.H., 1986. Fault-Zone Reactivation: Kinematics and Mechanisms. Philosophical Transactions of the Royal Society of London A: Mathematical, Physical and Engineering Sciences 317, 81-97.
White, S.H., Burrows, S.E., Carreras, J., Shaw, N.D., Humphreys, F.J., 1980. Shear zones in rocks On mylonites in ductile shear zones. Journal of Structural Geology 2, 175-187.
Younes, A.I., McClay, K., 2002. Development of accommodation zones in the Gulf of Suez-Red Sea rift, Egypt. AAPG Bulletin 86, 1003-1026.
Ziegler, P.A., 1992. North Sea Rift System. Tectonophysics 208, 55-75.

Figure Captions

Figure 1 - Figure showing the location of the study area (white box) in relation to offshore structural domains within the south eastern North Sea, as established through seismic interpretation. Structural domains are based upon the base Zechstein surface. Also shown is

909 the mapped onshore geology, taken from Fossen et al. (2014). The locations of major
910 Devonian shear zones onshore are shown in green.

911 **Figure 2** - Map showing the available datasets for use throughout this study; including 2D
912 and 3D seismic data, along with borehole data.

913 **Figure 3** - Stratigraphic framework within the study area showing the key seismic horizons
914 interpreted throughout this study, along with the major tectonic events to have affected the
915 region. Horizon colours are consistent and referred to throughout the text.

916 **Figure 4** – A) Panels showing the observed types of intrabasement reflectivity. 1) Shows the
917 observed thin intrabasement reflections packets, and 2) shows the thicker (Km-scale)
918 intrabasement packages. B) 1D waveform models of the observed reflection patterns.
919 Multiple models of layered sequences of varying thicknesses are created and then
920 subsequently compared to the observed reflection wavetrain. Individual layer thicknesses of
921 100 m, separated by 50-100 m produce the best match to the observed data.

922 **Figure 5** - Interpreted seismic section showing the large-scale structure and inter-
923 relationships between intrabasement structures. A series of steeply dipping structures can be
924 observed to cross-cut a relatively flat-lying structure. Inset – close-up of the cross-cutting
925 relationship observed in the centre of the image. See figure 1 for location.

926 **Figure 6** - Uninterpreted and interpreted seismic sections showing intrabasement structure
927 throughout the area. Larger intrabasement packages are shown in light grey with individual
928 thin intrabasement reflection packets highlighted by black dashed lines. Intrabasement
929 packages are mapped across the area, and linked along-strike to those shown in Figures 5, 7
930 and 8. A close-up of the right side of the image is shown in figure 10. Colours within the
931 sedimentary cover correspond to ages shown within the stratigraphic column (Figure 3) See
932 figure 1 for location.

933 **Figure 7** - Uninterpreted and interpreted regional seismic sections showing the geometry and
934 reactivation of intrabasement structure within the region. Intrabasement structures are
935 mapped across the area, and linked along-strike to those shown in Figures 5, 6 and 8. See
936 figure 1 for location.

937 **Figure 8** - Uninterpreted and interpreted seismic sections showing the regional intrabasement
938 structure in the south of the study area. A series of splays can be observed originating from
939 the base of IP4. See section 5 for details on the reactivation of these structures. See figure 1
940 for location.

941 **Figure 9** - Map showing the location of intrabasement structures across the study area.
942 Surface shown is the top acoustic basement time-structure map, highlighting the major
943 structural elements within the region, see figure 1 for more details. Also shown are the
944 locations of the structures as constrained by Fossen et al. (2014) (onshore and immediate
945 offshore locations), and Abramovitz and Thybo (2000) (Central North Sea). Note the
946 similarities in location between the intrabasement structures and the later rift-related faults.

947 **Figure 10** - Uninterpreted and interpreted seismic sections showing the location of the basal
948 décollement and associated Caledonian thrusts. A series of depocentres are observed in the
949 hangingwall of these structures, indicating extensional reactivation; some of which are
950 uplifted, indicative of later reverse reactivation. See figure 1 for location.

951 **Figure 11** - Uninterpreted and interpreted seismic sections highlighting multiple stages of
952 reactivation along the KSZ and FSZ beneath the Stavanger ramp area and. Seismic
953 stratigraphic relationships are used to constrain the timing of reactivation. See figure 1 for
954 location.

955 **Figure 12** - Uninterpreted and interpreted seismic sections showing the relationship between
956 the Åsta fault and the underlying KSZ, displaying a ‘merging’ type fault relationship. The

Åsta fault can be observed to sole onto the margin of the KSZ at depth. See figure 1 for location.

Figure 13 - Uninterpreted and interpreted seismic sections highlighting the interaction between the Sele High Fault System and the KSZ, displaying a 'cross-cutting' relationship. The SHFS can be observed to cross-cut the underlying KSZ. See figure 1 for location.

Figure 14 - Schematic models showing the 3 major types of interactions between intrabasement structures and rift-related faults. From left to right; Merging faults, Exploitative faults and cross-cutting faults.

Figure 15 - Synoptic figure showing how the presence of discrete intrabasement structures may modify the geometry and evolution of overlying rift systems. Upper panel shows pre-rift framework of structures within crystalline basement. Upon later extension these act to create localised perturbations in the regional stress field, producing a range of interactions with the rift-related faults.

Figure 1

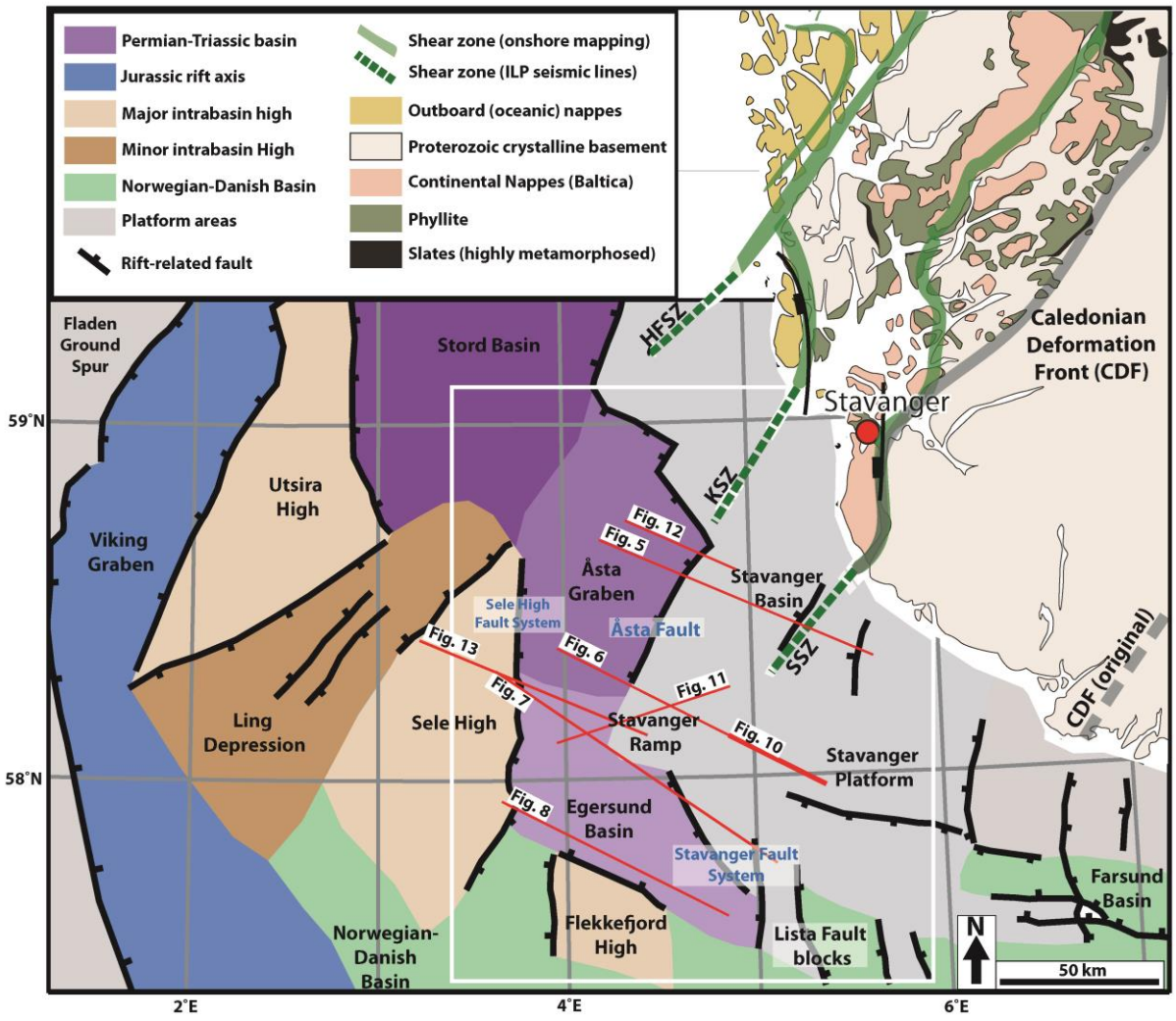
Permian-Triassic basin
Jurassic rift axis
Major intrabasin high
Minor intrabasin High
Norwegian-Danish Basin
Platform areas
Rift-related fault
Shear zone (onshore mapping)
Shear zone (ILP seismic lines)
Outboard (oceanic) nappes
Proterozoic crystalline basement
Continental Nappes (Baltica)
Phyllite
Slates (highly metamorphosed)
Fladen Ground Spur
Stord Basin
HFSZ
Caledonian Deformation Front (CDF)
Stavanger
59°N
KSZ
Utsira High
Viking Graben
Fig. 12
Fig. 5
Åsta Graben
Stavanger Basin
Sele High Fault System
Åsta Fault
Fig. 13
Fig. 6
SSZ
CDF (original)
Fig. 11
Fig. 7
Ling Depression
Sele High
Stavanger Ramp
Fig. 10
Stavanger Platform
58°N
Fig. 8
Egersund Basin
Stavanger Fault System
Farsund Basin
Norwegian-Danish Basin
Flekkefjord High
Lista Fault blocks
N
50 km
2°E
4°E
6°E

991 Figure 2

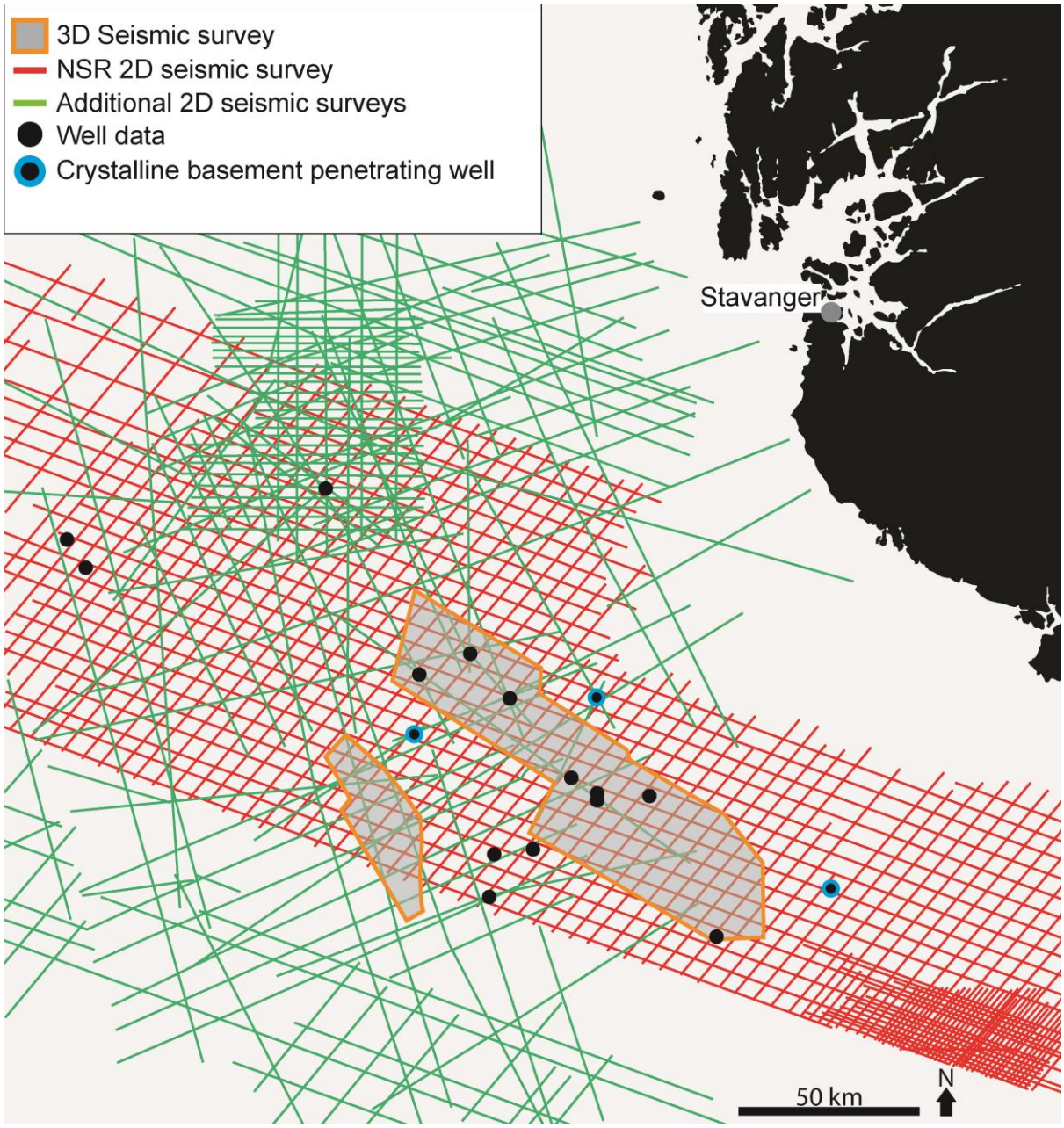

992

993

994

995

996

997

998

999

Figure 3

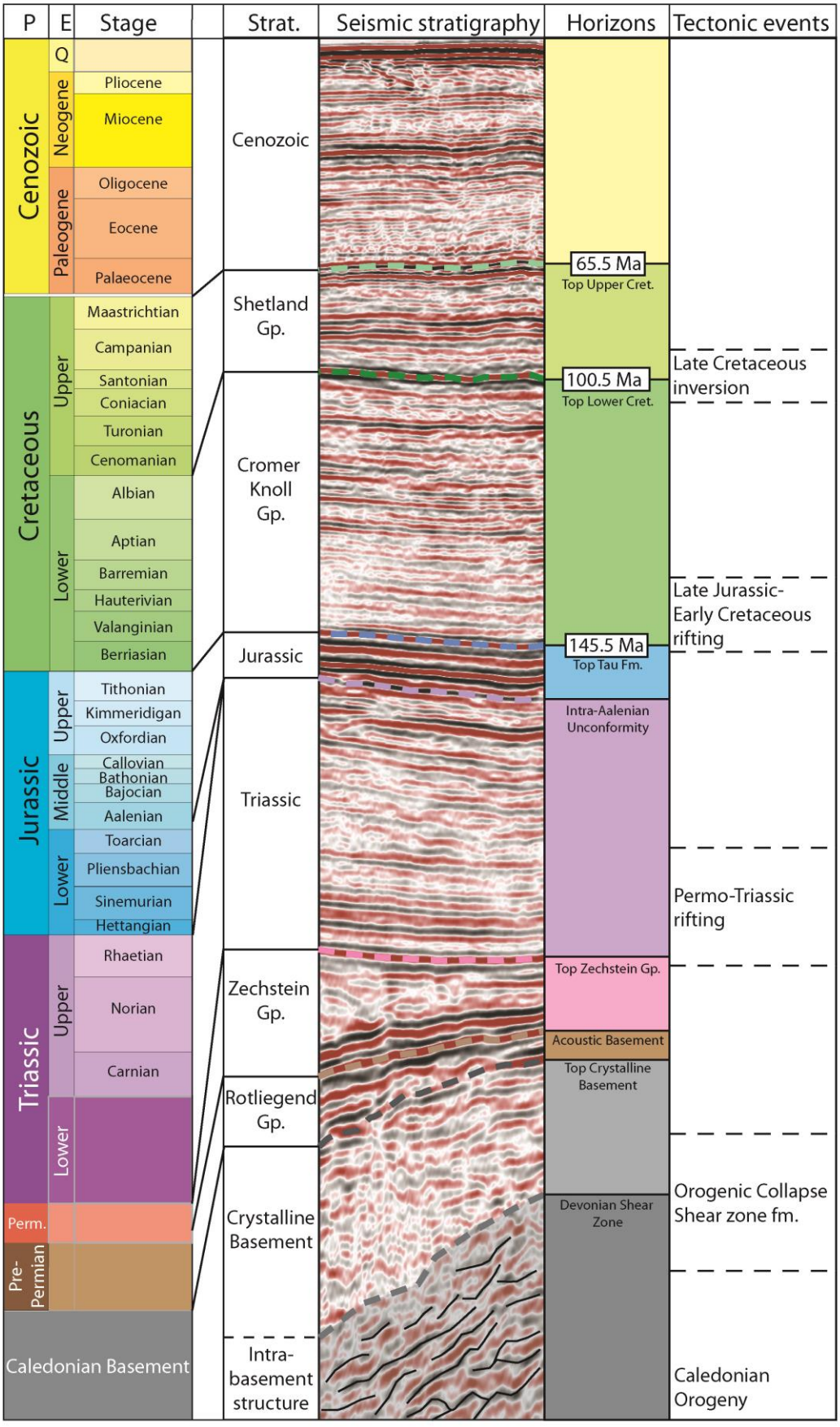
P
E
Stage
Strat.
Seismic stratigraphy
Horizons
Tectonic events
Cenozoic
Q
Neogene
Pliocene
Miocene
Paleogene
Oligocene
Eocene
Palaeocene
Cretaceous
Upper
Maastrichtian
Campanian
Santonian
Coniacian
Turonian
Cenomanian
Lower
Albian
Aptian
Barremian
Hauterivian
Valanginian
Berriasian
Jurassic
Upper
Tithonian
Kimmeridgian
Oxfordian
Middle
Callovian
Bathonian
Bajocian
Aalenian
Lower
Toarcian
Pliensbachian
Sinemurian
Hettangian
Triassic
Upper
Rhaetian
Norian
Carnian
Lower
Perm.
Pre-Permian
Caledonian Basement
Cenozoic
Shetland Gp.
Cromer Knoll Gp.
Jurassic
Triassic
Zechstein Gp.
Rotliegend Gp.
Crystalline Basement
Intra-basement structure
65.5 Ma
Top Upper Cret.
100.5 Ma
Top Lower Cret.
145.5 Ma
Top Tau Fm.
Intra-Aalenian Unconformity
Top Zechstein Gp.
Acoustic Basement
Top Crystalline Basement
Devonian Shear Zone
Late Cretaceous inversion
Late Jurassic-Early Cretaceous rifting
Permo-Triassic rifting
Orogenic Collapse Shear zone fm.
Caledonian Orogeny

1026 Figure 4

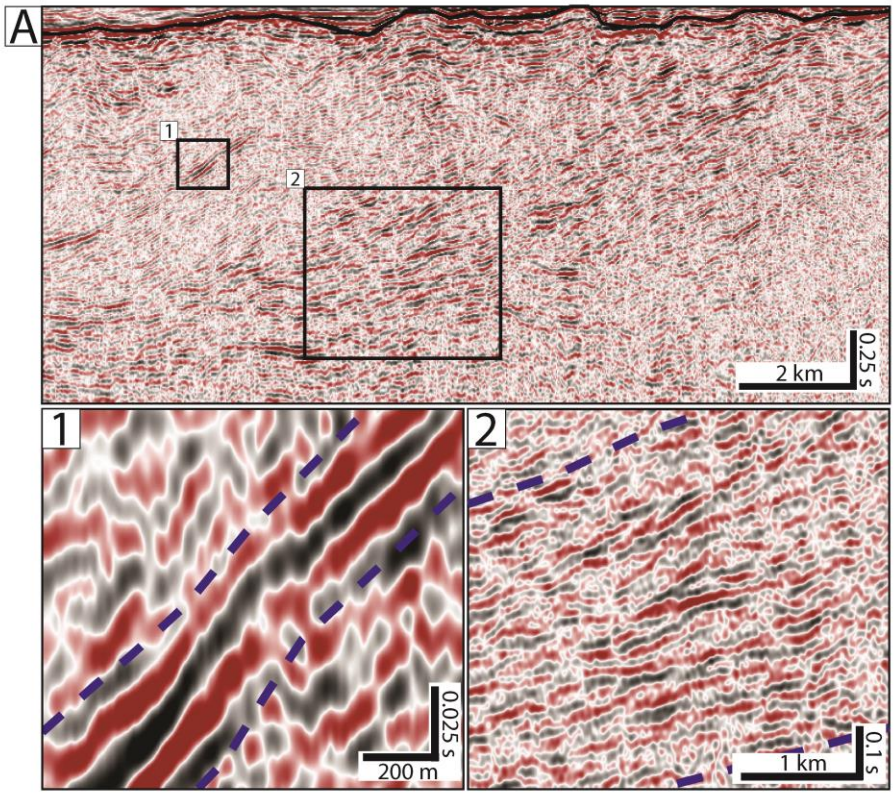

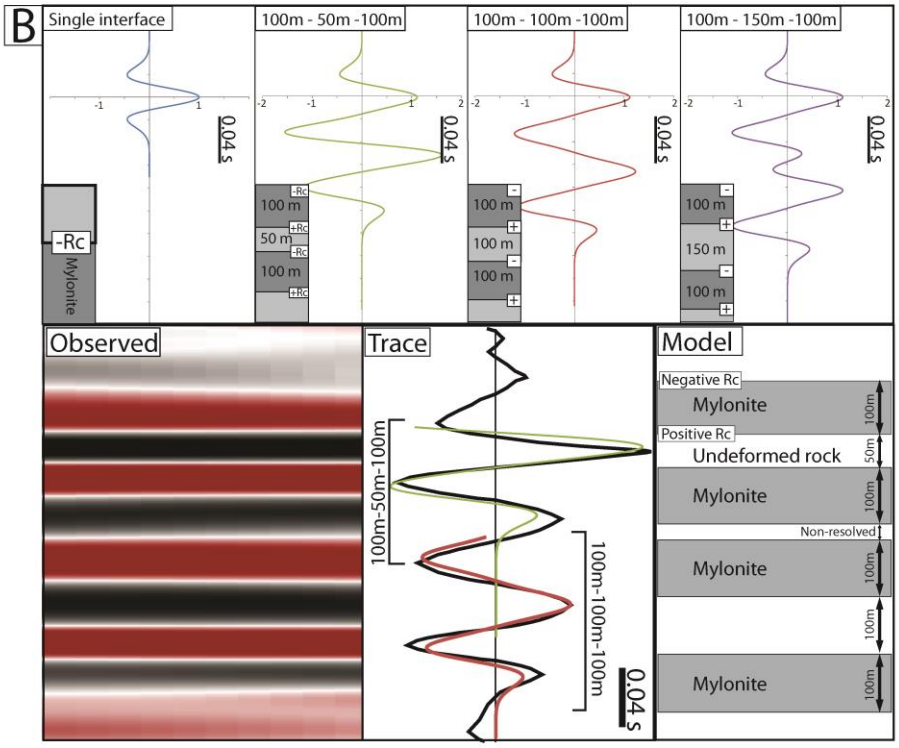

1027

1028

Figure 5

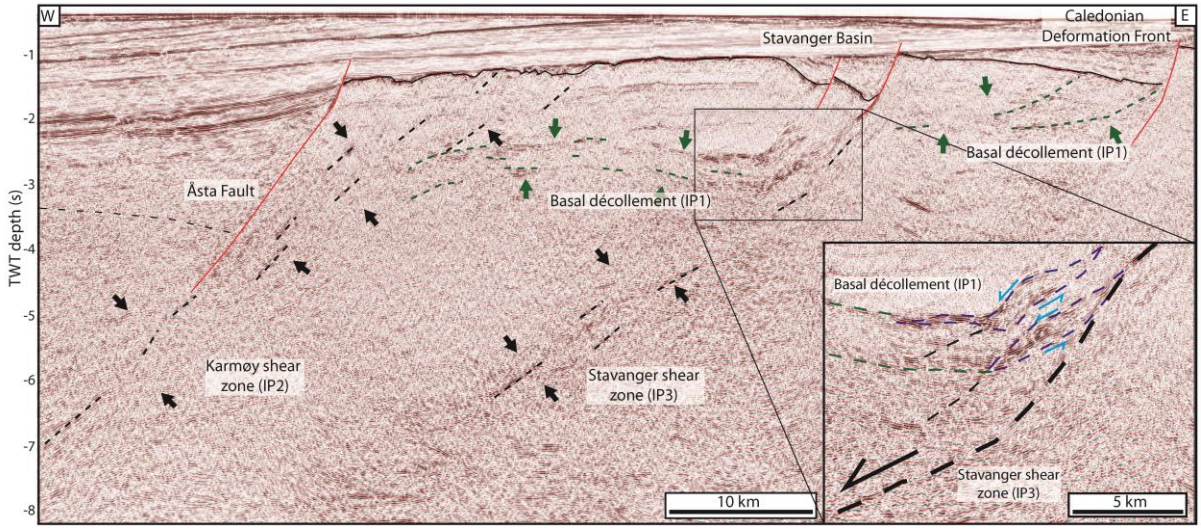

Figure 6

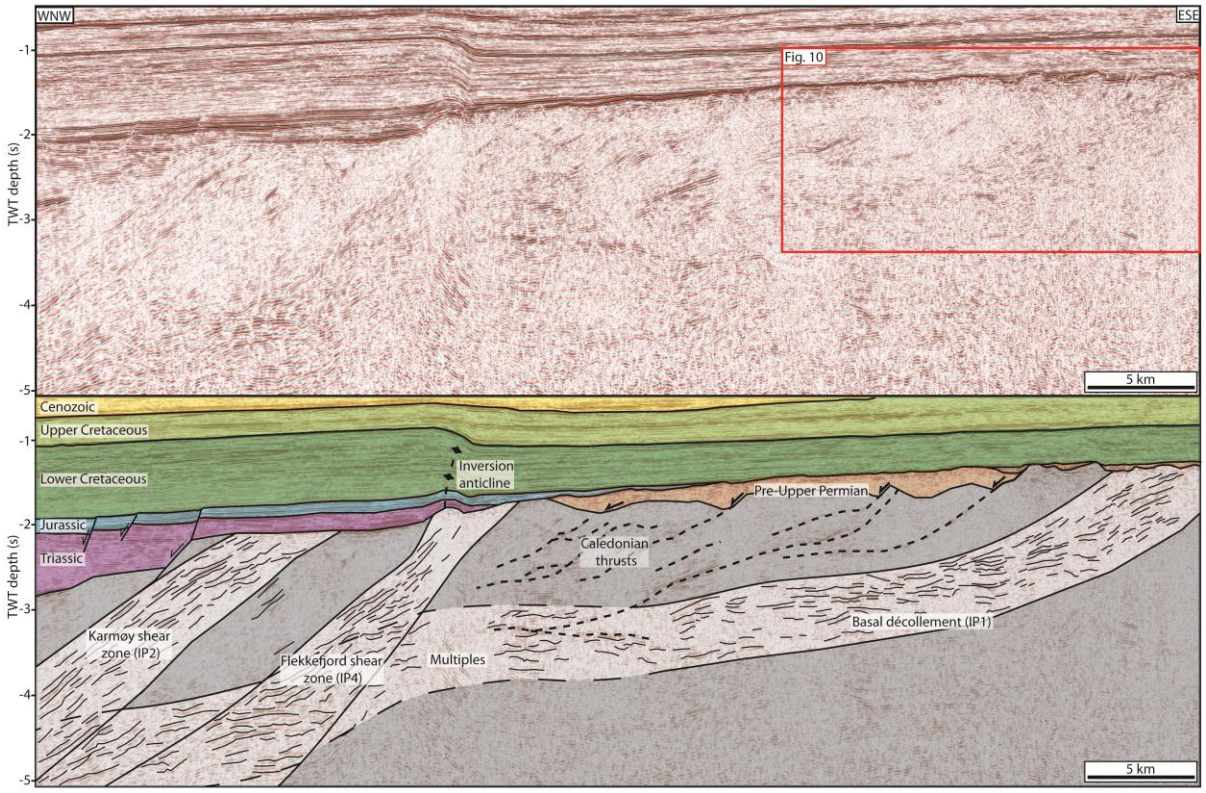

Figure 7

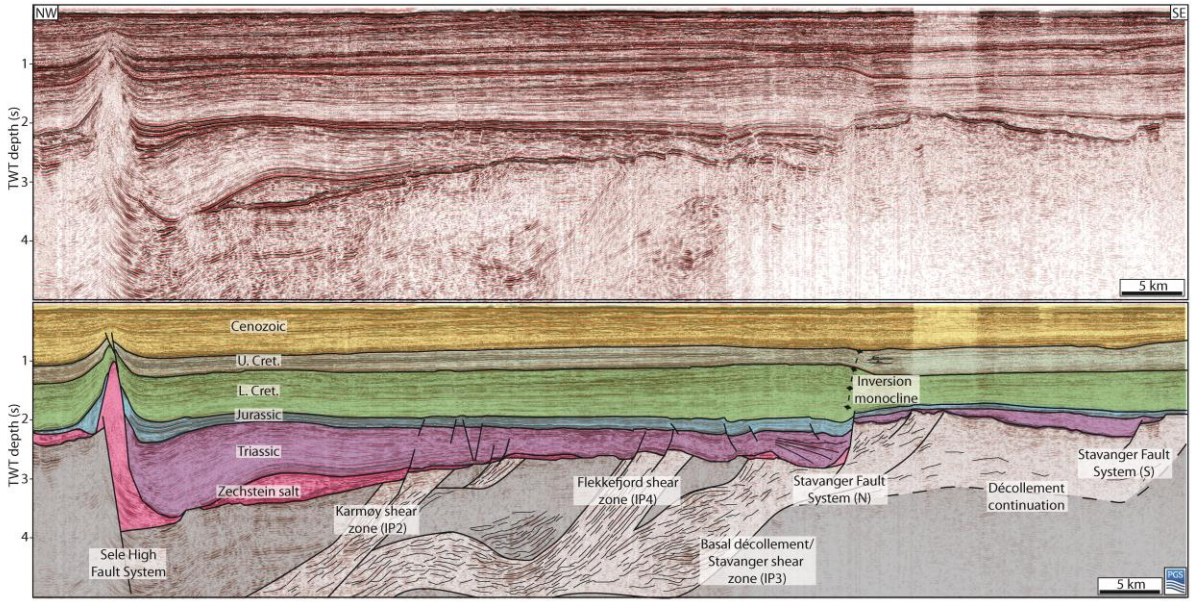

Figure 8

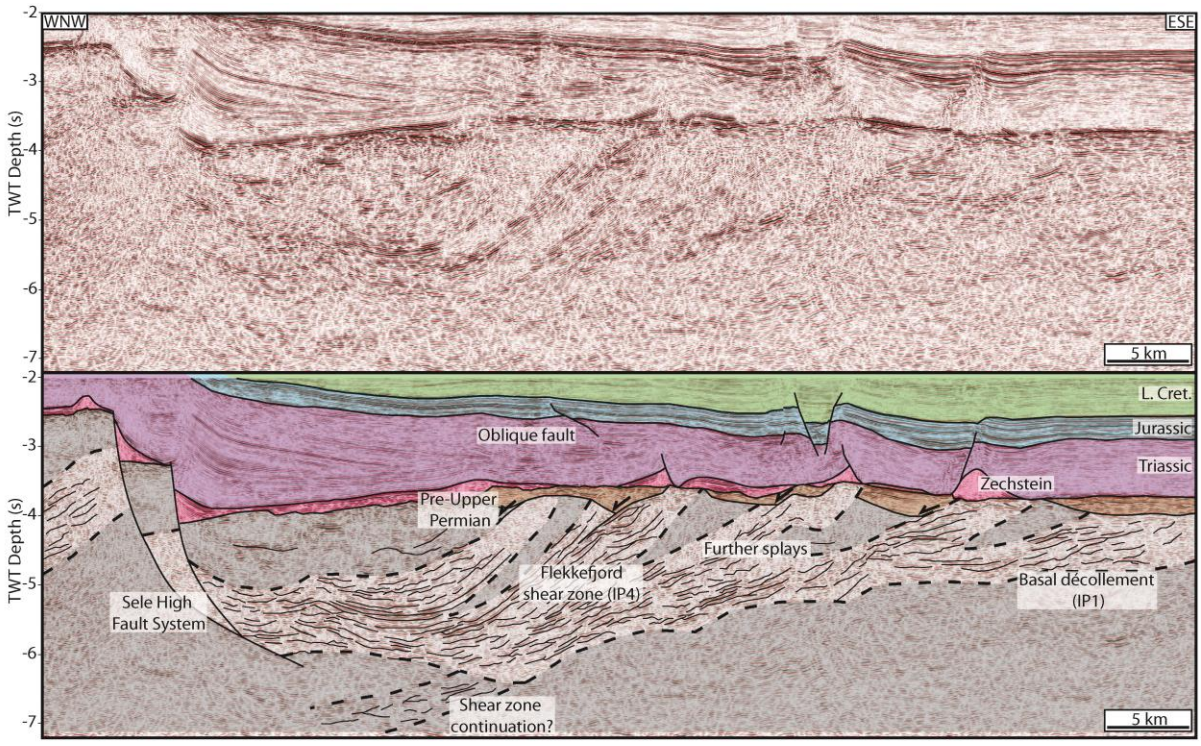

1047 Figure 9

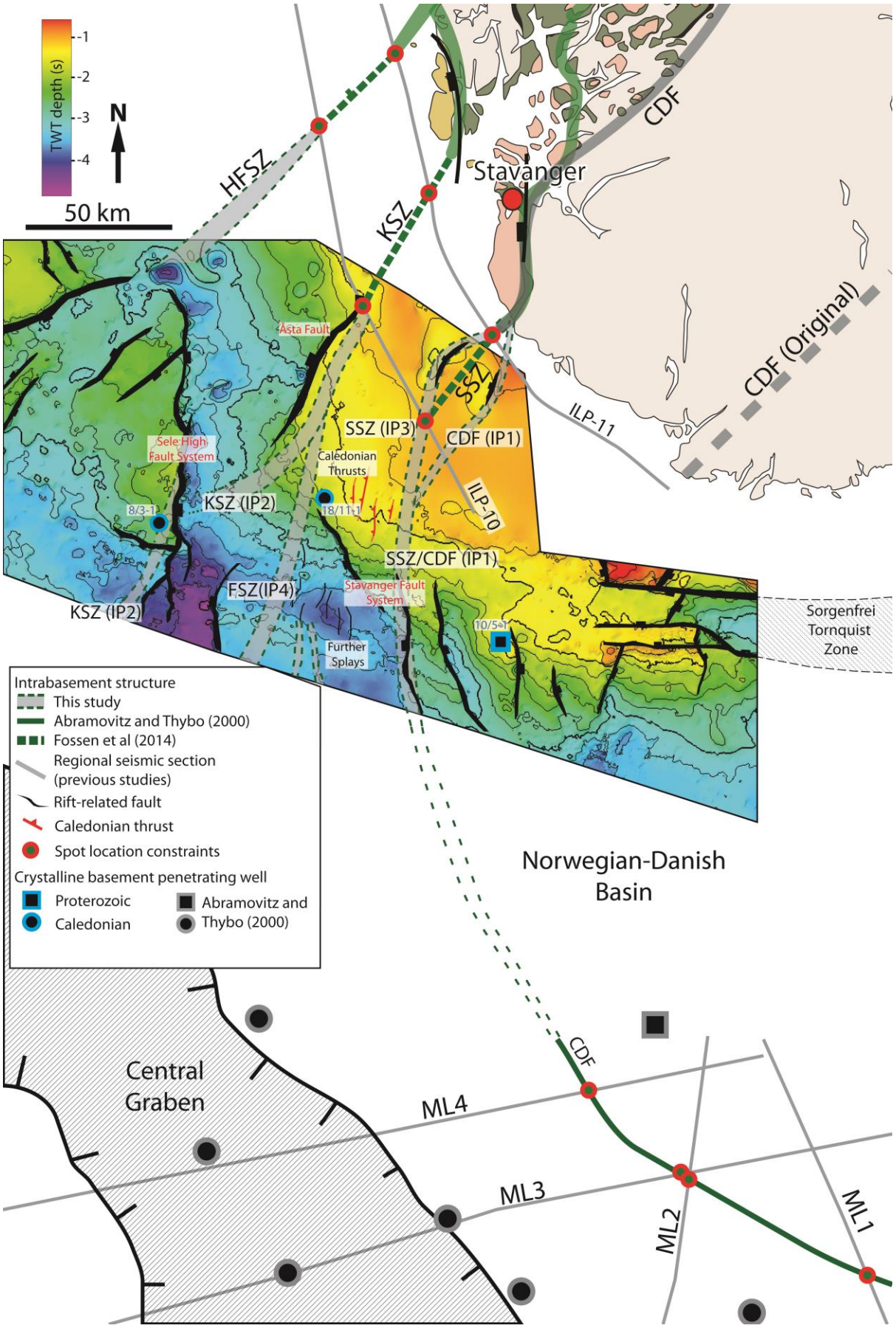

1048

Figure 10

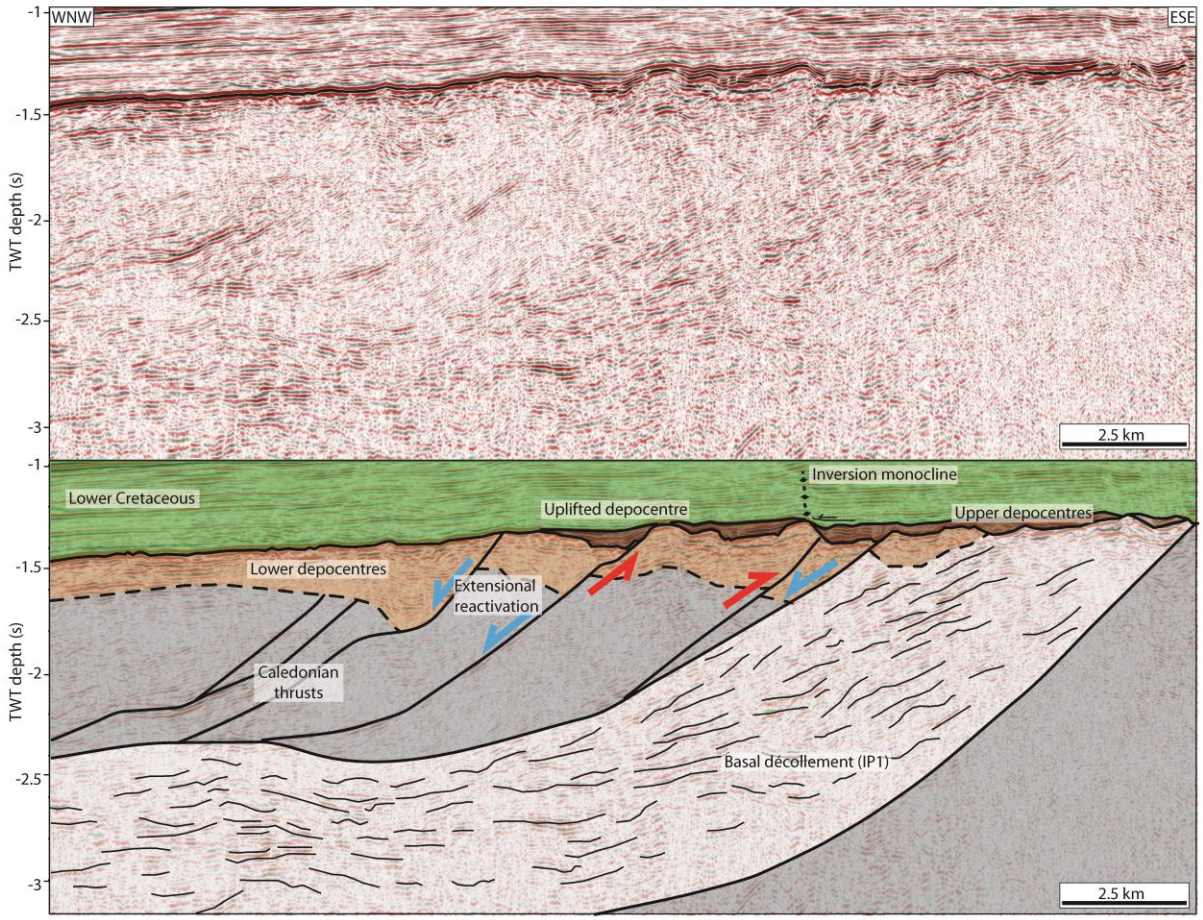

Figure 11

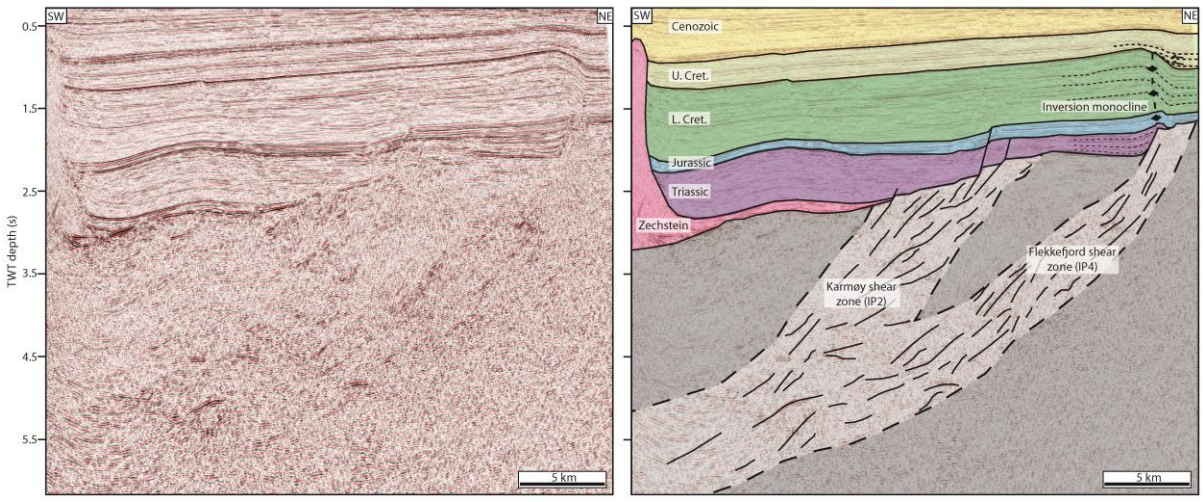

Figure 12

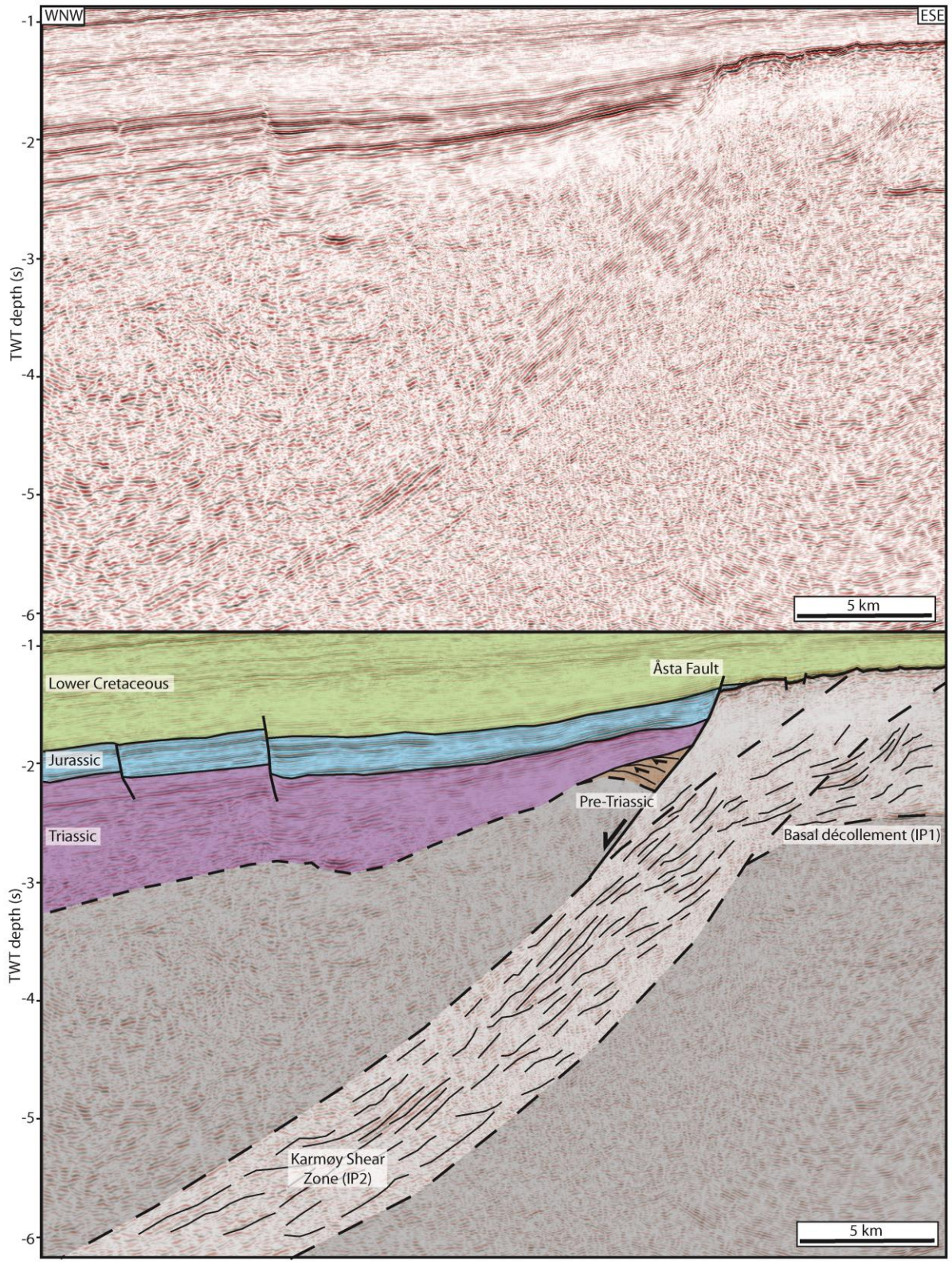
WNW
ESE
TWT depth (s)
-1
-2
-3
-4
-5
-6
5 km
Lower Cretaceous
Åsta Fault
Jurassic
Pre-Triassic
Triassic
Basal décollement (IP1)
Karmøy Shear Zone (IP2)
5 km

Figure 13

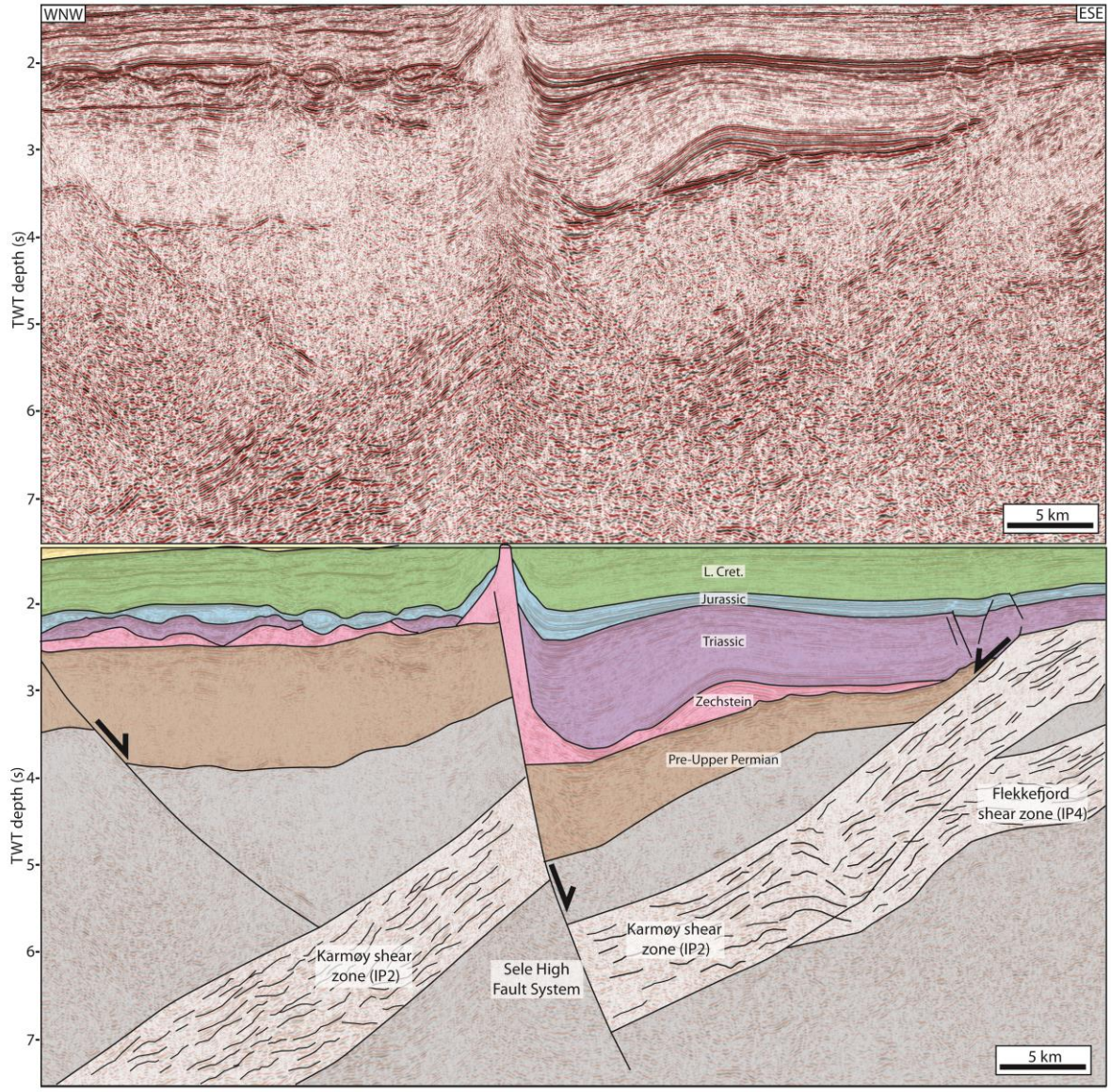
WNW
ESE
TWT depth (s)
2
3
4
5
6
7
5 km
L. Cret.
Jurassic
Triassic
Zechstein
Pre-Upper Permian
Flekkefjord
shear zone (IP4)
Karmøy shear
zone (IP2)
Sele High
Fault System
Karmøy shear
zone (IP2)
5 km

1069 Figure 14

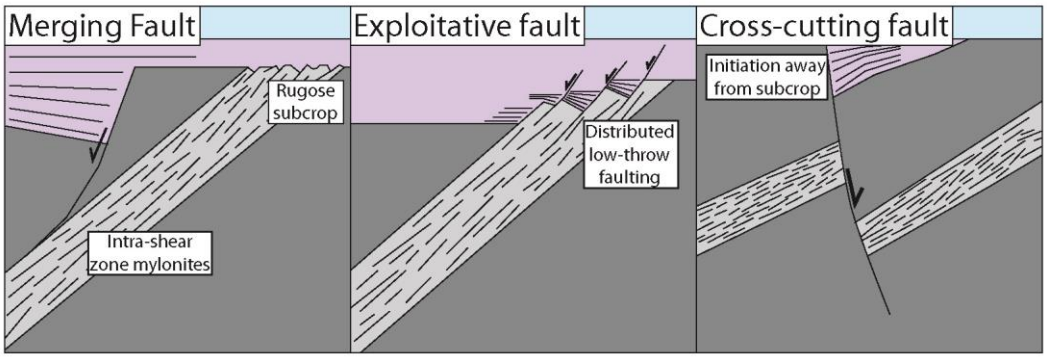

1070

1071 Figure 15

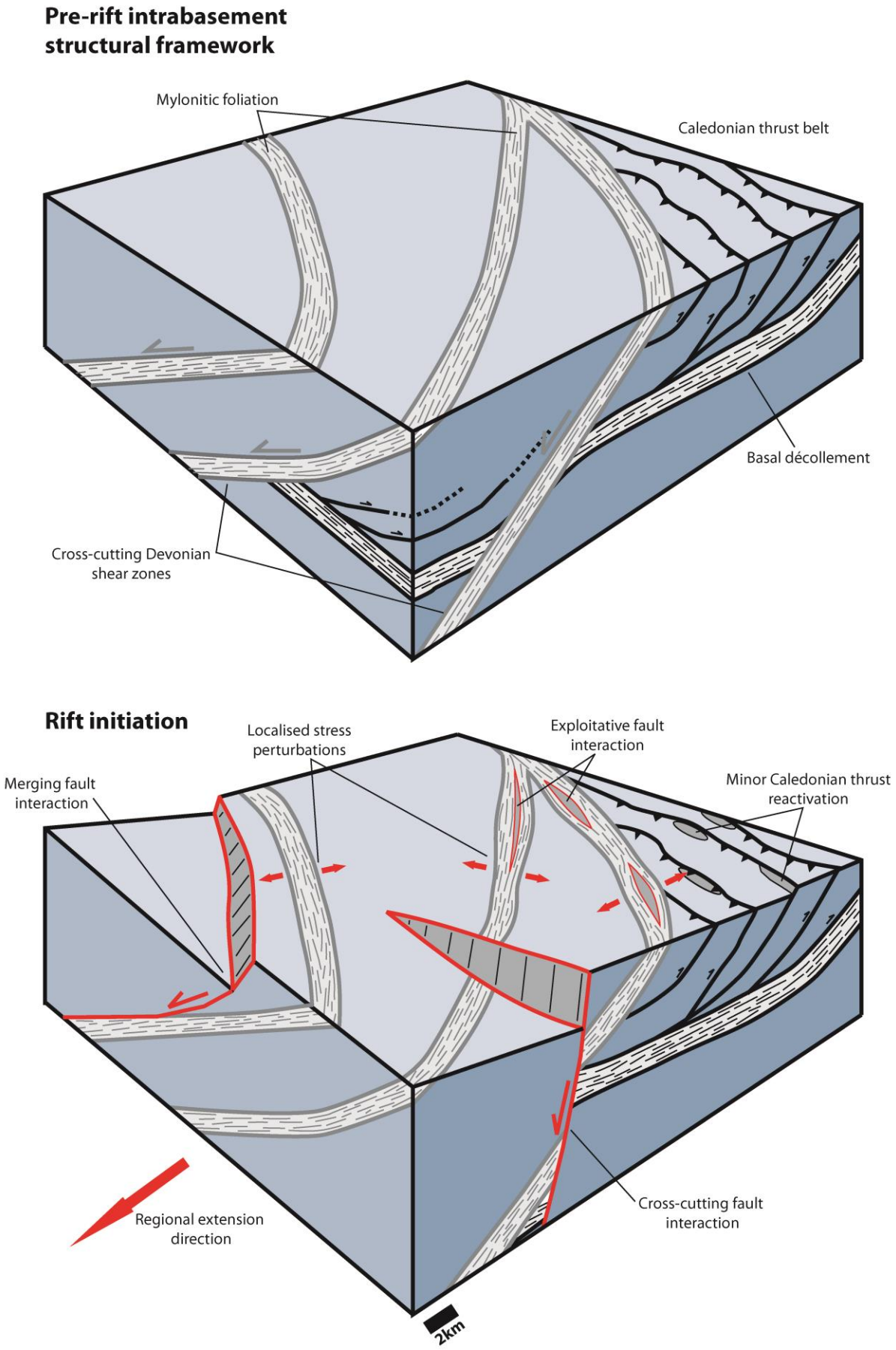

1072

1073

1074